# Phosphor Thermometry: Advances in Technique Development and Applications

Abou Nada, Fahed

2016

*Document Version:*
Publisher's PDF, also known as Version of record

# Phosphor Thermometry

## Advances in Technique Development and Applications

FAHED ABOU NADA | FACULTY OF ENGINEERING | LUND UNIVERSITY

# Phosphor Thermometry

## Advances in Technique Development and Applications

Fahed Abou Nada


LUND
UNIVERSITY

DOCTORAL DISSERTATION
by due permission of the Faculty of Engineering, Lund University, Sweden.

To be defended at Rydbergsalen, Fysicum, Professorsgatan 1, Lund. 9th of December 2016 at 09:15

*Faculty opponent*

Dr. Jeffrey Eldridge

NASA Glenn Research Center, USA

| Organization | Document name |
|---|---|
| LUND UNIVERSITY | Doctoral Dissertation |
| Division of Combustion Physics<br>Department of Physics<br>P.O Box 118, SE-211 00 Lund, Sweden | Date of issue<br>31 October 2016 |
| Author(s)<br>**Fahed Abou Nada** | CODEN<br>LUTFD2/TFCP-200-SE |

Title and subtitle: **Phosphor Thermometry: Advances in Technique Development and Applications**



Abstract

Understanding the mechanisms that govern the combustion processes is important for being able to further increase the efficiency of combustion devices. Temperature is considered to be one of the most important parameters controlling the progression and final products of combustion. Regulating the temperature in combustion devices enables higher degrees of efficiency to be achieved. The engine components in combustion devices are subjected to high levels of thermal load. These can strain many of the engine components and if it is unattended to can lead to catastrophic engine failure. Temperature information can help to assess the thermal load the engine is experiencing and as a result can increase the longevity of the engine while at the same time enabling higher levels of efficiency to be attained. In addition, the production of emission gases is closely correlated to the temperature present during the combustion of fuel. Comprehending the spatial and temporal distribution of temperature can aid in finding measures to reduce the levels of emission generated by a combustion engine.

Although several different temperature-probing techniques that can provide temperature information are available, the harsh and reactive nature of the experimental conditions present within combustion engines can severely limit the applicability of such techniques. Phosphor thermometry excels in delivering precise and accurate temperature information concerning harsh environments such as those present in combustion engines. It is a remote technique that is minimally intrusive and is highly robust. Phosphor thermometry utilizes the temperature-dependent characteristic emission of thermographic phosphors to retrieve temperature information concerning a surface or a fluid. The temperatures can be determined either on the basis of the temperature dependence of the decay time of the phosphorescence or on the basis of temperature-dependent changes in the spectral distribution of the phosphorescence.

The thesis presents the efforts that were made to develop the phosphor thermometry technique further. It involves demonstrations of use of this technique in combustion engines of different types. The results of the thesis work are reported in two major parts. In the first part, developments that were made in regard to certain fundamentals of the technique so as to improve its accuracy and precision are documented. This includes the development of an automatic calibration routine, a more precise characterization of the detector response, and investigation of the effects of engine lubricant oil on the performance of several different thermographic phosphors. The second part of the thesis reports on several applications of phosphor thermometry technique to remote probing of the temperature of different motor components, such as the piston, the cylinder wall, and the burner tip of the combustor. The overall aim of the work conducted was to improve the precision and the accuracy of decay time-based phosphor thermometry as well as to enhance its applicability under a wider range of experimental conditions than studied previously.



Key words: Phosphor thermometry, Laser-based combustion diagnostics, Decay time phosphor thermometry

Classification system and/or index terms (if any)

Supplementary bibliographical information | Language: English

| ISSN and key title: **1102-8718** | ISBN 978-91-7753-016-9 (Print) | ISBN 978-91-7753-017-6 (Electronic) |
|---|---|---|

| Recipient's notes | Number of pages 172 | Price |
|---|---|---|
| | Security classification | |




Signature 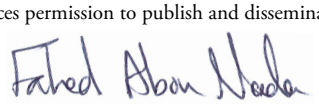 Date 31 October 2016

# Phosphor Thermometry

## Advances in Technique Development and Applications

Fahed Abou Nada


LUND
UNIVERSITY

Faculty and Department
ISBN 978-91-7753-016-9 (Print)
ISBN 978-91-7753-017-6 (Electronic)
ISSN 1102-8718
ISRN LUTFD2/TFCP-200-SE

Printed in Sweden by Media-Tryck, Lund University
Lund 2016




*"A mother is the truest friend we have, when trials, heavy and sudden, fall upon us; when adversity takes the place of prosperity; when friends who rejoice with us in our sunshine, desert us when troubles thicken around us, still will she cling to us, and endeavor by her kind precepts and counsels to dissipate the clouds of darkness, and cause peace to return to our hearts."*

*Washington Irving*

To my mother, my rock, my role model, my hero, and my very best friend.

# Abstract

Understanding the mechanisms that govern the combustion processes is important for being able to further increase the efficiency of combustion devices. Temperature is considered to be one of the most important parameters controlling the progression and final products of combustion. Regulating the temperature in combustion devices enables higher degrees of efficiency to be achieved. The engine components in combustion devices are subjected to high levels of thermal load. These can strain many of the engine components and if it is unattended to can lead to catastrophic engine failure. Temperature information can help to assess the thermal load the engine is experiencing and as a result can increase the longevity of the engine while at the same time enabling higher levels of efficiency to be attained. In addition, the production of emission gases is closely correlated to the temperature present during the combustion of fuel. Comprehending the spatial and temporal distribution of temperature can aid in finding measures to reduce the levels of emission generated by a combustion engine.

Although several different temperature-probing techniques that can provide temperature information are available, the harsh and reactive nature of the experimental conditions present within combustion engines can severely limit the applicability of such techniques. Phosphor thermometry excels in delivering precise and accurate temperature information concerning harsh environments such as those present in combustion engines. It is a remote technique that is minimally intrusive and is highly robust. Phosphor thermometry utilizes the temperature-dependent characteristic emission of thermographic phosphors to retrieve temperature information concerning a surface or a fluid. The temperatures can be determined either on the basis of the temperature dependence of the decay time of the phosphorescence or on the basis of temperature-dependent changes in the spectral distribution of the phosphorescence.

The thesis presents the efforts that were made to develop the phosphor thermometry technique further. It involves demonstrations of use of this technique in combustion engines of different types. The results of the thesis work are reported in two major parts. In the first part, developments that were made in regard to certain fundamentals of the technique so as to improve its accuracy and precision are documented. This includes the development of an automatic calibration routine, a more precise characterization of the detector response, and investigation of the effects of engine lubricant oil on the performance of several different thermographic

phosphors. The second part of the thesis reports on several applications of phosphor thermometry technique to remote probing of the temperature of different motor components, such as the piston, the cylinder wall, and the burner tip of the combustor. The overall aim of the work conducted was to improve the precision and the accuracy of decay time-based phosphor thermometry as well as to enhance its applicability under a wider range of experimental conditions than studied previously.

# Popular Science Abstract

Global energy consumption is continually increasing and despite the fact that renewable energy sources have increased their share of the globally generated energy, the majority of the energy produced comes from the combustion of fossil fuels. Since the 1970s, ever more stringent emission laws have been applied in efforts to reduce the production of air pollutants such as hydrocarbons, carbon monoxide, nitrogen oxides, sulfur oxide, particulate matter, and volatile organic compounds produced by combustion engines. Combustion engines are capable of transforming only a portion of energy contained in the fuel into useful work, the remainder of the energy being mostly lost as waste heat.

Instrumentation and experimentation are essential for developing combustion engines able to provide greater efficiency in the use of fuel and a reduction in the emissions produced. There is a variety of combustion-diagnostic techniques that provide insight into the combustion process as a whole through the information they make available concerning the chemical and thermal processes that take place during combustion. Many combustion-diagnostic techniques require the insertion or placement of physical probes within the test volume in order to obtain information of interest regarding such matters as temperature and chemical species concentrations. These techniques are intrusive in relation to the combustion process and thus can result in unreliable information being obtained. Through the utilization of laser radiation, laser-based combustion-diagnostic techniques are capable of delivering reliable and high quality information concerning the combustion process without interfering with the combustion process itself. Laser-based combustion-diagnostic techniques provide much needed information about fuel breakdown, fuel spray formation, chemical species concentrations, flow dynamics, and temperature to name just a few of the categories of information involved.

For the optimization of combustion within engines, attaining accurate and precise temperature measurements is essential. Temperature information pertaining to the various engine components sheds light on the different heat loss mechanisms involved, allowing for the development of better engine components that reduce the heat loss. Combustion devices such as car engines, gas turbines, and furnaces, impose severe demands upon the combustion-diagnostic techniques employed, making temperature measurement of high accuracy and high precision a very challenging task. Such difficulties as limited accessibility to the measurement volume, harshness of the test

environment, and chemical corrosiveness and strain due to different chemical and mechanical processes can render many temperature-measuring techniques virtually useless here.

Phosphor thermometry is a laser-based temperature sensing technique capable of providing accurate and precise temperature information from harsh environments such as those present in combustion engines. It also has many advantages that make it superior to other temperature measuring techniques. Phosphor thermometry is a remote sensing technique, meaning that temperatures can be measured without physical connections being needed, which is convenient when one is instrumenting reciprocating or rotating objects such as engine pistons and turbine blades. It is an accurate and precise temperature measurement technique that is capable of measuring temperatures ranging from room temperatures up to 1600 °C with a high degree of temporal and spatial resolution [1]. Phosphor thermometry is also robust under the experimentally challenging conditions usually found in combustion devices. However, it is important to also note that this technique suffers from certain disadvantages, such as its high level of complexity, its requirement of an optical access, and its high costs compared with many other techniques.

Phosphor thermometry utilizes temperature sensor materials known as thermographic phosphors in order to provide temperature measurement both on solid surfaces and in fluids. Thermographic phosphors exhibit a change in their characteristic luminescence as a result of changes in their temperature. Luminescence in thermographic phosphors can be induced by exposing them to excitation radiation that usually belongs to the ultraviolet part of the spectrum. The excitation radiation can be either continuous or in the form of pulses of very short duration. After excitation by a suitable type of radiation, thermographic phosphors most often emit a luminescence that is shifted in color to the visible part of the spectrum compared to the excitation radiation. The changes in luminescence that occur are exhibited in two different forms that can be employed for deducing from the thermographic phosphor the temperature information needed. In the first form, the relative intensity of the luminescence that is emitted increases in some parts of the spectrum but decreases in other parts. These relative changes in intensity can be utilized in order to deduce the temperature of the object that is instrumented. In the second form, after excitation by a short laser pulse (lasting a few billionths of a second) the emitted luminescence is long-lived and lasts much longer than the excitation pulse does. However, the intensity of the radiation that is emitted decays over time. The rate of decay can be used to deduce the temperature.

Phosphor thermometry technique provides information that can be highly useful in efforts to optimize the combustion processes involved and in the development of combustion engines generally. The thesis presents a summary of developments within the area of phosphor thermometry that have taken place and applications of it as a

remote temperature-sensing technique in combustion research. The developments in question have been aimed at improving the precision of the technique and characterizing various sources of error that can affect the temperature measurement so that one can obtain more reliable temperature information. Phosphor thermometry has also been employed with success for measuring temperatures in combustion engines of various sorts, such as marine engines, large diesel engines, and gas turbines. The work of this sort carried out here represents a collaboration of different groups and persons from universities, from industry and from government agencies in efforts to improve the efficiency of the energy production that combustion engines can provide.

# List of Papers

I. *Development of an Automatic Routine for Calibration of Thermographic Phosphors*
F. Abou Nada, C. Knappe, X. Xu, M. Richter, and M. Aldén
Measurement Science and Technology, **25**, 025201 (2014)

II. *On the Automation of Thermographic Phosphor Calibration*
F. Abou Nada, C. Knappe, X. Xu, M. Richter, and M. Aldén
The 60th International Instrumentation Symposium Conference Proceedings, 4.1.1 (2014)

III. *Comparison of Photo Detectors and Operating Conditions for Decay Time Determination in Phosphor Thermometry*
C. Knappe, F. Abou Nada, M. Richter, and M. Aldén
Review of Scientific Instruments, **83**, 094901-10 (2012)

IV. *Improved Measurement Precision in Decay Time-based Phosphor Thermometry*
F. Abou Nada, C. Knappe, M. Aldén, and M. Richter
Applied Physics B, **122**, 1-12 (2016)

V. *Investigation of the Effect of Engine Lubricant Oil on Remote Temperature Sensing Using Thermographic Phosphors*
F. Abou Nada, M. Aldén, and M. Richter
Journal of Luminescence, **179**, 568-573 (2016)

VI. *A First Application of Thermographic Phosphors in a Marine Two-Stroke Diesel Engine for Surface Temperature Measurement*
F. Abou Nada, J. Hult, C. Knappe, M. Richter, S. Mayer, and M. Aldén
ASME 2014 Internal Combustion Engine Division Fall Technical Conference Proceedings, **ICEF 2014-5417**, V001T01A001 (2014)

VII. *Remote Temperature Sensing on and Beneath Atmospheric Plasma Sprayed Thermal Barrier Coatings Using Thermographic Phosphors*
F. Abou Nada, A. Lantz, J. Larfeldt, N. Markocsan, M. Aldén, and M. Richter
Surface and Coatings Technology, **302**, 359-367 (2016)

# Related Work

*I.* *Investigation and Compensation of the Nonlinear Response in Photomultiplier Tubes for Quantitative Single-Shot Measurements*
C. Knappe, J. Linden, F. Abou Nada, M. Richter, and M. Aldén
Review of Scientific Instruments, **83**, 034901-7 (2012)

*II.* *Response Regime Studies on Standard Detectors for Decay Time Determination in Phosphor Thermometry*
C. Knappe, F. Abou Nada, J. Lindén, M. Richter, and M. Aldén
AIP Conference Proceedings, **1552**, 879-884 (2013)

*III.* *Sprays Thermometry Using Two Color LIF and SLIPI*
Y. N. Mishra, S. Polster, F. Abou Nada, E. Kristensson, and E. Berrocal
The 13th International Conference on Liquid Atomization and Spray Systems Proceedings, 1-8 (2015)

*IV.* *Thermometry in Aqueous Solutions and Sprays Using Two-Color LIF and Structured Illumination*
Y. N. Mishra, F. Abou Nada, S. Polster, E. Kristensson, and E. Berrocal
Optics Express, **24**, 4949-4963 (2016)

# Contents

# 1 Introduction

Pollutants such as particulate matter, nitrogen oxides, sulfur oxides, and ozone lead to deaths caused by air-pollution in the form of such diseases as lung cancer, or respiratory infections, or of strokes and ischaemic heart disease. It is estimated that some 7 million premature deaths annually are attributable to exposure to air pollution. According to World Health Organization, air pollution is now considered to be the world's largest single environmental health risk [2]. The levels of pollutants are still increasing, despite the stringent emission laws pertaining to power generation and the transportation sector that are enforced. Even with the reduction that has occurred in the emission levels produced per energy unit involved, the increasing global energy demand has led to a rise in the pollutant levels around the globe. Although the share of such renewable energy sources as wind power and hydropower is likewise growing, combustion-based power generation represents the largest portion of the global energy production. Such fuels as diesel, gasoline, coal, natural gas, and fuels of other types are consumed by internal combustion engines or boilers in combustion processes for producing the power that is needed. The higher the fuel consumption rates are, the higher the emission levels become. Through optimizing the efficiency of engines, one can reduce the amounts of fuel needed to generate a given amount of energy, while at the same time producing lesser emissions. One report concludes that the reduction in particulate matter concentration from 70 microgram per cubic meter ($\mu g/m^3$) to 20 $\mu g/m^3$ results in some 15% less air-pollution-related deaths [3]. It is thus of the utmost importance to reduce the emissions generated through optimizing the combustion processes taking place within combustion engines.

To improve the efficiency of combustion engines used in transportation and in power generation, we need to possess information of high quality regarding the combustion processes that lead to the production of energy and of pollutants. Combustion is a complex process, one that entails a multitude of sub-processes that interact and that control the progress and the products of the combusted fuel. Sub-processes such as those of chemical kinetics, fluid dynamics, heat transport, vaporization, energy exchange and transformation are intertwined and are difficult to separate. All of these processes occur simultaneously, which indicates that any alteration in one process translates into a change in the accompanying processes and eventually a global change in the combustion-process behavior as a whole. Obtaining information regarding the factors controlling these processes, such as the concentrations of different

chemical species, flow field velocities, pressure, and temperature with a desired spatial and temporal resolution is essential in the development of the comprehension of the combustion process. Information concerning fuel concentrations and fuel-air ratios can provide insight into how the soot obtained is formed. Knowledge of the concentration of different chemical species helps one understand the chemical reactions occurring and the chemical pathways leading to the formation of the different pollutants that develop. The physical dynamics of the combustion process, as portrayed by the complex transport mechanisms involved, affect both the chemical reactions that occur and the heat transfer that takes place within the engine. The temperatures that are present control to a considerable degree the different combustion sub-processes occurring, their measurement aiding in the study of the chemical kinetics and the heat transport that are necessary for combustion engines to be optimized.

Versatile and robust measurement techniques are required in order to obtain high quality quantitative and qualitative information regarding the combustion process. Techniques such as hot wire anemometer, thermocouples, and mass spectrometry by sample probing, provide information regarding fluid flows, temperatures, and the abundance of different chemical species. These techniques, due to their inherent features, can perturb the measurement volume and lead to biases in the measured values which can compromise the quality of the data obtained. With the introduction of lasers, new laser-based combustion-diagnostic techniques emerged. Laser-based combustion diagnostics employ different types of laser radiation sources to non-intrusively probe the combustion processes involved and to retrieve information regarding fluid dynamics, chemical species concentration distributions, fuel spray development, temperature and many other matters [4]. Laser-based combustion-diagnostic techniques include such techniques as laser-induced fluorescence, laser-induced incandescence, laser-induced phosphorescence, absorption spectroscopy, coherent anti-stokes Raman scattering, particle image velocimetry, laser Doppler velocimetry, Rayleigh/Raman scattering, and laser-induced phosphorescence, to name just a few of them [5]. All of these techniques are capable of delivering highly spatially and temporally resolved information in zero, one, two, or three dimensions, and also time-resolved three dimensional information. High spatial and temporal resolution mean that the complex chemical, thermal, and fluid dynamics involved can be observed clearly to help us explain the different elements of the combustion process. Chemical reactions in combustion are extremely fast, occurs during periods of as short as one trillionth of a second, which requires the use of lasers with ultrafast pulses that can 'freeze' the chemical reactions involved and provide insight into the chemical mechanisms that are present. The present thesis reports on the development and application of one particular laser-based diagnostic technique that is phosphor thermometry.

# 2 Temperature Sensing Techniques

Temperature is one of the most frequently measured parameters. Information concerning the temperature of a system or an object is essential to gaining an understanding of its properties. In combustion engines, temperature controls the different combustion processes and determines the operation lifetime expectancy of an engine. Knowing the surface temperature of the different engine components can help in determining the thermal loads the engine components are subjected to under different operating conditions. In addition, temperature data contain an abundance of information that is a key to developing engines of high efficiency. There a large variety of techniques that are capable of delivering temperature information concerning a given probed system. These techniques are often categorized in terms of their being invasive, semi-invasive, and non-invasive techniques, respectively [6]. The selection of the temperature-measuring technique that is most appropriate depends upon a number of prerequisites, such as those of availability, robustness, the environment involved, cost, response, stability, temperature range, sensitivity, accuracy, and probing method employed. In this section, a few temperature measurement techniques will be described and be compared in respect to their potential in different applications for use as temperature measurement methods for combustion diagnostic purposes. The techniques described here are categorized in terms of the nature of the contact present between the sensor and the surface of interest into contact techniques and remote techniques. Contact techniques are temperature measurement techniques that require that there be a direct physical contact between the sensor and the system the temperature of which is to be measured. These techniques also require leads from the sensor to the acquisition/readout device that retrieves the temperature values obtained. Whereas remote techniques, are concerned with changes that occur either in the luminescence that is emitted from the measurement volume or object or in luminescence that originates from a thin layer of an optically activated material.

## 2.1 Contact Techniques

The contact techniques described in this section are thermocouples and resistance temperature detectors (RTDs). Both techniques are well established and widely used in multitude of applications. Both techniques exploit the dependence of the electrical

properties of metallic materials and their alloys on the temperature that is present. Thermocouples use the electromotive force produced by a circuit of two different conductors whereas RTDs uses changes in the electrical resistance of certain metals to deduce the temperature.

### 2.1.1 Thermocouples

Thermocouples are widely used as devices for temperature measurement. Their simplicity, low cost, and robustness make them highly desirable as temperature sensors in various applications. If the junctions of two dissimilar conductors are held at different temperatures, a potential is created across their terminals. This is a thermoelectric effect known as the Seebeck effect. The potential that is generated (in terms of volts) is proportional to the difference in temperature between the two conductors at their junction. Thermocouples are usually made of an alloy from different metals. The properties of a thermocouple namely its temperature range, its maximum temperature, and its resistance to oxidation depends upon the materials used to create the thermocouple. Thermocouples are capable of measuring temperatures ranging from -270 up to 3000 °C [6].

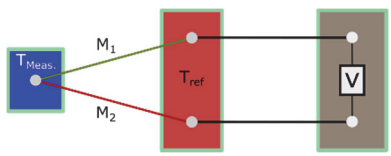


*Figure 2.1 The working principle of a thermocouple*

Thermocouples have numerous advantages such as their low cost, high degree of accuracy, and robustness as compared with other methods, as well as their ability to measure a wide range of temperatures. Thermocouples are also capable of providing a relatively fast response time to the changes in temperature involved [7]. Thin-film thermocouples, approximately 3 - 4 µm thick, have been developed for use in temperature sensing within internal combustion engines [8, 9]. The increased time response of thin-film thermocouples usually comes at the cost of reduced robustness, especially under high-speed and high-load operating conditions [10]. Thermocouples also suffer from limitations in terms of their use on moving surfaces. The fact that thermocouples require wires to carry and deliver the potential that is generated, limits their use in connection with reciprocating and rotating objects. However, when telemetric systems are employed, thermocouples can be used on or in reciprocating and rotating objects at the cost of higher levels of error in the temperature measurements obtained. Another major limitation is the degree of alteration, in both thermal and chemical terms, that the physical presence of a thermocouple subjects the measured

system to. In combustion environments such as those found in engines, the presence of a thermocouple biases the temperature of the object of interest. In addition, it can act as a chemical catalyst that can alter the chemical reactions taking place during combustion.

### 2.1.2 Resistance Temperature Detectors

Resistance temperature detectors (RTD) are devices that utilize the resistance of a conducting element to determine the temperature. The temperature can be determined through knowing how a change in resistance is related to a change in temperature. Depending on the conductor material used, temperatures up to 950 °C can be measured [6]. Platinum, copper, and nickel are the mostly used material in the manufacturing of RTDs.

RTDs are highly accurate and are widely used in industrial applications. Similar to thermocouples, their requirement on physical contact with the object of interest can lead to measurement biases. RTDs can also suffer from a phenomenon called self-heating, which is due to the power dissipation leading to an erroneous temperature reading.

RTDs are more expensive than thermocouples and have a lower degree of robustness than the latter do. The major advantage that thermocouples have over RTDs is the wide range of temperatures they can encompass. However, temperature readings of RTDs are superior in terms of accuracy and repeatability.

## 2.2 Remote Techniques

Contact temperature instrumentation techniques can suffer from degradation in environments that are very high in temperature and are chemically damaging. Remote techniques in contrast, do not suffer from such limitations, making them more suitable for instrumentation in instrumentally challenging environments. Remote temperature instrumentation techniques such as infrared thermography and phosphor thermometry enable accurate and precise temperature determination to be obtained with minimum intrusiveness. Remote sensing techniques utilize information available in the radiation emitted from the environment or from an optically active sensor. The emitted radiation is captured by a photo-sensor, such as a camera or a photomultiplier tube, which converts the radiation into an image or an electric signal.

### 2.2.1 Infrared thermography

Every material emits radiation, the intensity of which is positively relative to the absolute temperature of the material. The wavelength of the radiation that is emitted, known as thermal radiation, depends upon the temperature of the object. Thermal radiation is emitted in a wavelength range extending from 0.1 to 100 μm [6]. Infrared pyrometry measures the radiation emitted in a range that extends from 0.7 to 20 μm, due to limitations in the sensitivity of the detector.

Pyrometers and infrared-cameras are the most widely used infrared temperature sensing devices. They measure the irradiance (J) of the target and deduce the temperature in accordance with the Stefan-Boltzmann law; see Equation 2.1.

$$J = \varepsilon \sigma T^4 \qquad \text{Equation 2.1}$$

T here is the temperature, σ is the Stefan-Boltzmann constant, and ε is the emissivity of the target. The emissivity is defined as the ratio of the energy emitted by an object at one temperature to the energy emitted by a black-body object at the same temperature. Since the emissivity of most objects diverges from that of a black-body, it is necessary to know the emissivity of the target object in order to determine the temperature correctly. The emissivity of various materials can display a dependence upon the temperature of the emitting object, thus making the calibration of the emissivity a necessity. Through the use of ratio pyrometry, in which the ratio of one spectral band to the other is utilized to determine the temperature, the dependence of emissivity upon the temperature involved can be canceled out. If the emissivity of the target material exhibits a variation with respect to the observed wavelength, then multi-band (3 or more bands) pyrometry need to be used to account for variations in emissivity and to attain accurate readings [11].

The remoteness of infrared thermometry techniques enables the user to perform temperature measurements on moving objects. Infrared thermometers are compact in size and simple to operate, and are application-unspecific, making them highly desirable for all sorts of temperature-sensing purposes. Infrared thermometers are capable of measuring temperatures ranging between -50 up to 4000 °C. Despite their advantages, their application is limited to measuring the temperature of surfaces only. Optical access to the target object is needed to retrieve the temperature. The accuracy of the temperature readings obtained can deteriorate if dust and smoke are present in the measurement medium. Since they measure the thermal radiation received, infrared thermometers are susceptible to biases introduced by spurious radiation produced by flames. They fail to differentiate between the infrared radiation originating from the target and the infrared radiation originating from another object and is reflected off the target object.

### 2.2.2 Phosphor Thermometry

Phosphor thermometry is another temperature-sensing technique, one that is capable of determining the temperature remotely through use of sensor materials known as thermographic phosphors. Unlike infrared thermometry techniques which are non-invasive, phosphor thermometry is semi-invasive, since it requires the deposition of a sensor layer on the target object. This deposited sensor layer has a thickness of only 10 to 20 micrometers, providing negligible degree of intrusiveness to the probed system.

Thermographic phosphors are usually composed of a host material and an activator. The activator, usually a rare-earth metal, optically activates the host and converts it into a light emitter when it is excited by suitable radiation. Most thermographic phosphors emit radiation in the visible part of the electromagnetic spectrum. They are usually excited effectively by ultraviolet (UV) radiation. The luminescence emitted by thermographic phosphors displays variations as a function of changes in their temperature. The changes observed can take the form of changes in the spectral density of the spectrum which is emitted or of temporal changes in the delayed emission of them, the latter being termed phosphorescence. Thermographic phosphors are capable of measuring temperatures ranging from cryogenic temperatures up to 1600 °C.

Phosphor thermometry can deliver temperature information with a high degree of temporal and spatial resolution. High temporal and spatial resolution are highly desirable when measuring temperatures in systems with high temperature gradients in order to resolve the temperature changes and attain a full understanding of the occurring thermal processes. Phosphor thermometry has a high degree of precision, even at high temperatures. It also exhibits a high degree of robustness when it is employed in demanding combustion environments. Unlike thermocouples and RTDs, the remoteness of this technique eliminates the need of telemetry systems when it is applied to rotating or reciprocating objects. As with all optical sensing techniques, phosphor thermometry requires optical access to the target object. Optical fibers and other forms of waveguides have been used to deliver the excitation radiation that is needed and to retrieve the emitted luminescence.

An experienced operator is needed if phosphor thermometry is to be carried out with a minimum of errors. This technique is also high in cost as compared with other temperature-sensing techniques such as thermocouples. Despite these limitations or drawbacks, phosphor thermometry is highly desirable, due to all of the advantages that have been referred to.

# 3 Experimental Equipment

In applying phosphor thermometry to an object or a flow, the thermographic phosphor in question is first excited by suitable radiation. The emitted radiation is then collected by an optical system composed of lenses and interference filters. The collected luminescence is filtered spectrally is then projected onto a photodetector. In the present section, the excitation source used for optically exciting the thermographic phosphors employed within the thesis work is described. In addition, several different types of photodetectors and the characteristics they possess are presented.

## 3.1 Light Sources

The excitation source used can vary between continuous and pulsed, depending upon on the phosphor thermometry method employed. For the decay time method, pulsed excitation radiation sources are usually employed to resolve the decay time of the phosphorescence that is emitted. The decay time of a thermographic phosphor can also be determined by use of a high-frequency sinus-modulated excitation radiation. The decay time is calculated then from the phase shift exhibited by the emitted phosphorescence.

Low excitation fluence is usually needed in order to excite the thermographic phosphor employed. This enables excitation sources other than pulsed lasers such as LEDs and laser diodes to be implemented instead, as low cost alternatives to use of pulsed lasers as excitation sources.

Pulsed and continuous excitation sources can be implemented in use for the intensity ratio method. All of the work presented here utilized radiation that was generated by an Nd:YAG laser for exciting the thermographic phosphors that were tested.

### 3.1.1 Pulsed Nd:YAG Lasers

Nd:YAG lasers are solid-state lasers capable of delivering high-energy pulses. The fundamental wavelength of Nd:YAG lasers is 1064 nm. Through utilizing harmonic

generators to double the frequency or to mix the fundamental frequency with the doubled frequency, enables laser radiation at 532, 355, and 266 nm to be obtained. A Q-switched Nd:YAG laser provides a laser pulse that is few nanoseconds wide in the temporal regime with spatial profile close in its appearance to a Gaussian distribution.

A Pulsed Nd:YAG laser was utilized in all of the work presented in the thesis. The Nd:YAG system has a repetition rate of 10 Hz. The generated pulse has a diameter of 9 mm and a temporal width at half maximum of 6 ns. This system is capable of delivering 400 mJ, 150 mJ, and 90 mJ at 532 nm, 355 nm, and 266 nm, respectively. High laser energy densities are beneficial when large surfaces are to be illuminated especially when the intensity ratio is employed over large surfaces. Caution is necessary to avoid laser-induced heating and phosphor saturation.

## 3.2 Detectors

Photodetectors convert the incident photonic input signal into an electrical output signal that can be acquired by a signal acquisition unit and be processed later for extracting of the information that is needed. Several types of photodetectors were employed in the work reported in the thesis work. All of the detectors employed were of the point-detector type that ranged among photomultiplier tubes (PMT), micro-channel plate PMTs, and avalanche photodiodes. Each detector type has its characteristic conversion mechanism, as well as an inherent sensitivity and signal-magnification capability.

### 3.2.1 Photomultiplier Tube

A photomultiplier tube is a vacuum tube composed of a photocathode, as well as focusing electrodes, a dynode chain, and an anode (Figure 3.1). Light that impinges upon the PMT window hits the photocathode, which converts the incident photons into photoelectrons by a process known as the photoelectric effect. The photoelectrons are then emitted into the vacuum of the tube. Focusing electrodes accelerate and focus the generated photoelectrons then towards the surface of the first dynode. Upon impact, the photoelectrons are multiplied in a process known as secondary emission. Multiplication by secondary emission is repeated at each dynode in the chain, leading to a multiplication factor of $10^6$ to $10^7$. The secondary electrons emitted by the last dynode are then collected by the anode and an output signal is produced.

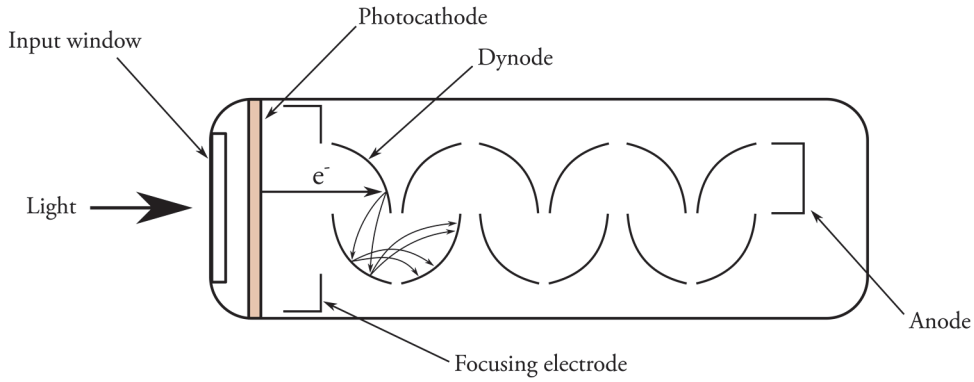


*Figure 3.1 Sketch of a head-on type photomultiplier tube.*

The spectral sensitivity range of a PMT is determined by the type of photocathode material employed. Photomultiplier tubes can be time-gated, which enables the PMT to accept radiation only in a predetermined time window that is determined by an input gating pulse. Time gating is achieved by applying a voltage bias to the photocathode with respect to the focusing electrode and the first dynode. If a reverse bias is applied, any photoelectrons that are emitted are unable to reach the first dynode and to multiply as they would during regular operations. When a forward bias is applied to the photocathode, the generated photoelectrons accelerate towards the dynode chain and normal operations then take place. An extensive description of the PMT components and its operating characteristics is available in the PMT handbook published by Hamamatsu Photonics [12].

### 3.2.2 Micro-channel Plate Photomultiplier Tube

A micro-channel plate (MCP) PMT, as the name suggests, utilizes an MCP plate so as to multiply the electrons emitted from the photocathode rather than utilizing a dynode chain, as in the case of a regular PMT. The incidence of photons upon the photocathode leads to the release of photoelectrons. The photoelectrons are then directed towards the micro-channel plate for the multiplication process to proceed. The micro-channel plate is composed of a bundle of thin glass tubes about 6 to 20 μm in diameter, each tube acting as a separate electron multiplier (Figure 3.2). When an electron impinges upon the MCP channel wall, secondary electrons are emitted. The emitted secondary electrons are accelerated by means of the high voltage applied across the MCP. The accelerated secondary electrons impinge on the wall of the micro-channel repeatedly, releasing further electrons. At the end of the MCP, the electrons that are generated are then collected by the anode and an output signal is produced. MCP-PMTs are characterized by their short response times (in the order of

picoseconds) and their high gain. MCP-PMTs can also be time-gated by switching the MCP voltage on and off. MCP-PMTs have a gain factor of up to $10^6$ to $10^7$ similar to that of the regular PMTs.

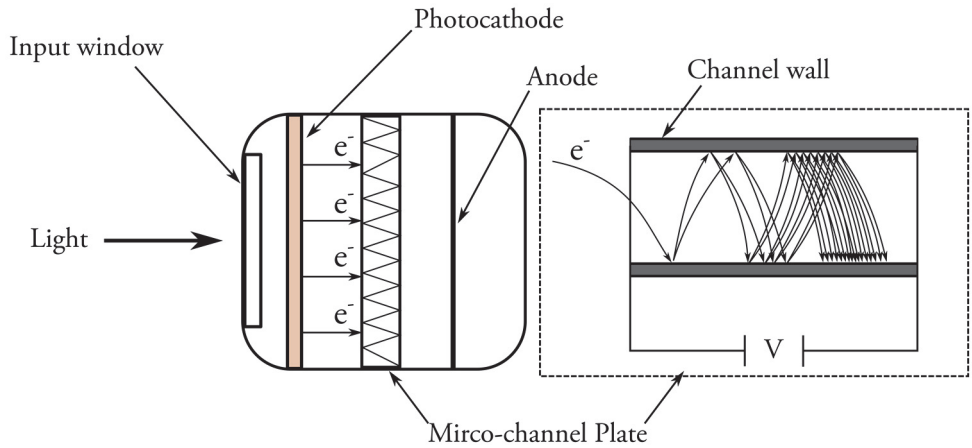


*Figure 3.2 Sketch of a micro-channel plate photomultiplier tube.*

### 3.2.3 Avalanche Photodiodes

Avalanche photodiodes (APDs) are a semiconductor type of photodetectors that convert the light input into an electric output signal. APD utilizes a multiplication mechanism known as avalanche multiplication. When a photon of sufficient energy hits the APD surface, an electron–hole pair is created in the depletion layer of the APD. If a reverse voltage bias is applied to the PN-junction of the APD, the holes involved accelerate towards the N-side of the junction while the electrons accelerate towards the P-side of the junction. As the reverse voltage is increased, the drift speeds of the electrons and the holes increase and their corresponding kinetic energy build up. If an electron or a hole collides with the crystal lattice of the junction, a new electron-hole pair is generated. The newly generated pair also accelerates and collides with the crystal lattice, creating new pairs. This, known as the avalanche effect, is responsible for the gain of the APD that occurs. The gain of the APD is directly proportional to the reverse voltage that is applied. In most cases, APDs have reverse voltages ranging from 100 to 200 V and a gain ranging from 10 to 1000. Silicon APDs are sensitive to light extending from the UV to the infrared part (200 to 1000 nm range) of the spectrum. APDs are sensitive and reliable detectors but have much lower gain capabilities than PMTs and MCP-PMTs do, which limits their application under low signal conditions. Under very low signal-level conditions, PMTs and MCP-PMTs outperform APDs.

# 4 Phosphor Thermometry

Phosphor thermometry utilizes materials known as thermographic phosphors (TPs) in order to provide temperature information concerning an object or a fluid. Phosphors are described as being thermographic when one or more of their luminescence properties show a sensitivity to temperature changes. Thermographic phosphors have been used since the middle of the last century as temperature sensors and have been employed since then in a multitude of applications. The dependence of the emission intensity or the decay time on the temperature provides the temperature sensing capability of thermographic phosphors. The present chapter describes the luminescence mechanism of thermographic phosphors and the methodology needed to implement the temperature-dependent decay time and the luminescence intensity so as to deduce the temperature of the thermographic phosphor that is employed. In addition, factors that can influence the phosphor luminescence, such as saturation effects, impurities, dopant concentration, and pressure are also described.

## 4.1 Thermographic Phosphors

### 4.1.1 Principles of TP Luminescence

Thermographic phosphors are usually inorganic materials that are mainly composed of a host and an activator. The host, such as aluminum oxide and oxysulfides, is usually optically inactive when irradiated by UV radiation. Doping the host by use of activators leads to luminescence being emitted by the composite material. The activator thus makes the mixture optically active, it usually radiates electromagnetic radiation extending over the visible range of the spectrum. The activators involved usually belong to the rare-earth elements known as lanthanides such as Eu, Tb, Dy, and Er, to name a few. If the activator ions exhibit a low degree of absorption of the excitation energy, impurities known as sensitizers can be added so as to enhance the luminescence generated by the activator ions. Sensitizer ions absorb part of the excitation energy and transfer it to the activator ions which then emit the transferred energy into a photon. Sensitizers can also emit a photon instead. This can be noted in some cases in the emission spectra of thermographic phosphors in which sensitizer ions

have been incorporated. Some sensitizers can also display an emission sensitivity to temperature. Figure 4.1 illustrates the process of energy absorption and emission within a luminescent material (such as TPs) that possesses both activator and sensitizer ions. Upon excitation by a suitable radiation, the activator atoms (A) are promoted from the ground state to the excited state, after which the energy is emitted in the form of a stoke-shifted photon or through thermal dissipation or a combination of both.

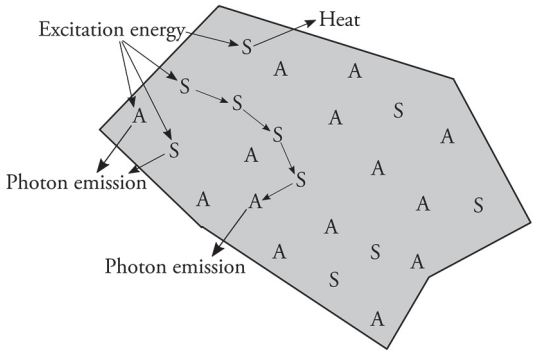


*Figure 4.1 An illustration of the absorption of excitation energy and emission of the subsequent radiation by activator ions (A) and sensitizer ions (S).*

Rare-earth elements have a particular electronic configuration that can be clearly seen in the produced luminescence. Emission spectra from rare-earth elements are characterized by sharp spectral lines. The sharpness of the spectral lines is due to the fact that the *4f*-shell of rare-earth elements is shielded by the filled *5s*-shells and *5p*-shells, $La^{3+}$ and $Lu^{3+}$ being an exception to this. Due to the shielding of the 4f-shell electrons, the host crystal field has a negligible effect on the position of these levels. The resultant emission from incorporated rare-earth ions contained in solids resembles that of the free ions. In lanthanides, luminescence is generated due to $4f^n$-$4f^n$ transitions, $4f^n$-$4f^n5d$ transitions, and charge transfer transitions.

There is a variety of processes that occur which determine the result of the absorption of an excitation photon. Figure 4.2 shows the possible pathways the excitation energy can take after excitation by an incident photon. Upon the absorption of an excitation photon, an electron is promoted from the ground state to the excited state (1), after which the electron de-excites to the lowest vibrational level of the excited electronic state through non-radiative energy transfer (2). A transition to the electronic ground state (3) results in the emission of a stoke-shifted photon as distinguished from the excitation photon. Subsequent non-radiative energy transfer through vibrational relaxation demotes the electron to the lowest vibrational level of the ground state (4). At sufficiently high temperatures, while the electron is still in the excited state, thermal activation can promote the electron's passing of the intersection point of the ground and excited state potentials (5). This results in non-radiative de-excitation, through

thermal dissipation, of the electron back to the ground state (6). In some rare-earth elements (such as $Eu^{3+}$), a charge transfer state (CTS) plays a major role in the process of energy transfer and emission. CTS can enhance the emission intensity either by transferring energy from neighboring atoms to the emitting atom or by quenching the emission through enhancing non-radiative energy transfer pathways. The energy level configurations and the corresponding transitions of many thermographic phosphors are discussed in detail in several sources [13-15].

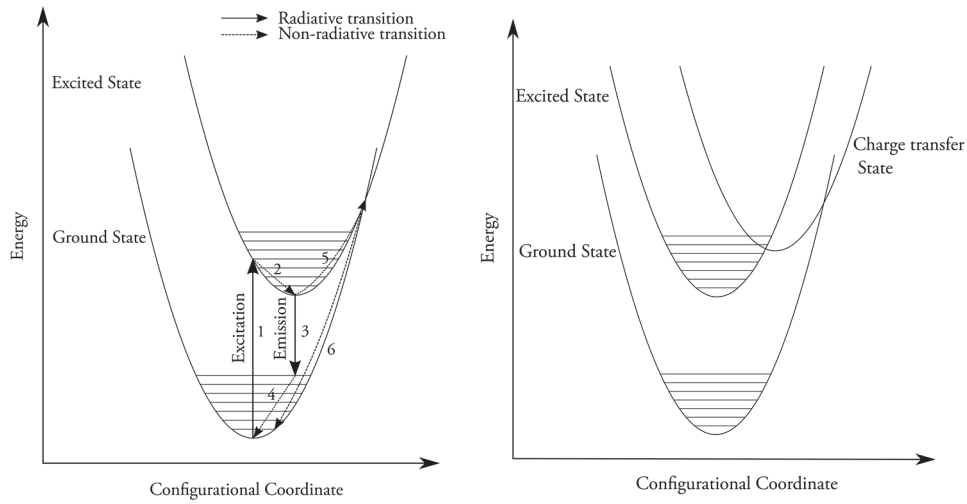


*Figure 4.2 A configurational coordinate diagram showing the electronic transitions that occur in luminescent materials upon excitation by incident radiation.*

The persistence of luminescence after excitation is known as after-glow. Depending upon the temporal length of the after-glow, the luminescence can be categorized either as fluorescence or as phosphorescence. This distinction is not universal, both terms being used interchangeably in various fields of study. The persistence of the emission involved can be attributed to the forbidden nature of the transitions that take place. The emission intensity as function of time, after termination of the excitation, can be approximated by a single exponential function, such as shown in Equation 4.1.

$$I(t) = I_0 e^{-t/\tau} \qquad \text{Equation 4.1}$$

Where $I(t)$ is the emission intensity at a specific time $t$ after the excitation termination, $I_0$ is the emission intensity at time $0$ after the excitation, and $\tau$ is the decay time of the luminescence. The number of excited luminescence centers (N*) is

determined by the radiative ($Q_R$) and non-radiative ($Q_{NR}$) transition probabilities as described in Equation 4.2.

$$\frac{dN^*}{dt} = -(Q_R + Q_{NR})N^* \qquad \text{Equation 4.2}$$

The solution of this equation is an exponential function:

$$N^*(t) = N_0^* e^{-(Q_R+Q_{NR})t} \qquad \text{Equation 4.3}$$

The decay time of the luminescence center can be expressed as

$$\tau = {}^{1}/_{(Q_R + Q_{NR})} \qquad \text{Equation 4.4}$$

The quantum efficiency ($\eta$) can be expressed as a function of the radiative and non-radiative transition probabilities

$$\eta = {}^{Q_R}/_{(Q_R + Q_{NR})} \qquad \text{Equation 4.5}$$

The radiative transition probability is defined as the collective spontaneous emission probabilities from the emitting upper level to all of the final states. Non-radiative relaxation mechanisms can be generalized as consisting of two seperate processes.

The first process, known as thermal relaxation, requires that thermal activation occur. At sufficiently high temperatures, ions in the excited state can gain energy that permits non-radiative relaxation to occur through the crossing-point between the potential parabolas of the lower and of the higher electronic states (Figure 4.2). The probability of center relaxation through thermal activation is given by Equation 4.6.

$$A = ce^{-\varepsilon/kT} \qquad \text{Equation 4.6}$$

Where $\varepsilon$ is the thermal activation energy, k is the Boltzmann constant, T is the temperature, and c is a rate constant ($s^{-1}$).

The second non-radiative relaxation mechanism is through multi-phonon emission. It usually occurs when no cross-point exists. Multiple phonons are emitted then to fill the gap created by the difference in energy ($\Delta E$) between the upper and the lower level. As the temperature increases, the non-radiative transfer rates increase, the decay time and the emission intensity decrease correspondingly.

### 4.1.2 Factors Affecting TP Luminescence

Several factors can impede or alter the luminescence intensity and the decay time of the thermographic phosphor employed for temperature sensing. Effects such as those of dopant concentration, luminescence saturation, impurities and pressure can change the performance of a thermographic phosphor dramatically.

#### *4.1.2.1 Dopant Concentration*

When using rare-earth elements for doping a host material, dopant concentrations ranging of around few percent are usually employed. Dopant concentration affects the luminescence intensity, the spectral distribution, the decay time, and the temperature sensitivity of the thermographic phosphor. Most thermographic phosphors have an optimal dopant concentration, one that provides the strongest emission intensity and temperature sensitivity. At concentrations higher than the optimal dopant concentration, the probability of energy transfer between the different dopant sites increases, leading to concentration quenching. Concentration quenching leads to a reduction in the luminescence which is produced, due to energy being dissipated into the host lattice. Changing the dopant concentration affects the corresponding decay time of the thermographic phosphor.

#### *4.1.2.2 Luminescence Saturation*

Subjecting various thermographic phosphors to high fluxes of excitation energy can lead to luminescence saturation. When such saturation occurs, the luminescing material no longer generates an increase in emission intensity as a function of the increase in excitation energy. Saturation not only affects the quantum efficiency of the thermographic phosphor, but it also alters the rise and the decay times of the corresponding phosphorescence. Saturation of the 543 nm emission line from $Y_3Al_5O_{12}$:Tb (YAG:Tb) has been studied and has been attributed to the depletion of the ground state and the interaction of two excited activator ions [16]. That study also concluded that a high activator concentration leads to lower saturation effects and prolonged the luminescence linearity to higher excitation energies. The saturation mechanisms in $Zn_2SiO_4$:Mn (the 505 nm emission line) and in YAG:Tb (419 and 515 nm emission lines) were studied by de Leeuw et al. [17]. That study indicates that as the excitation energies increase, the decay time decreases as compared with the decay time at low energies and the decay temporal profile displays a non-exponential behavior. A study of $Y_2O_2S$:Eu saturation revealed that the addition of Pr or Tb dopants, even at the very low concentrations, diminished the observed saturation [18].

#### *4.1.2.3 Impurities*

Impurities in thermographic phosphors, even at ppm levels, can impede the quantum efficiency of the emitted luminescence and the corresponding decay time. Impurities absorb part of the excitation radiation and emit radiation that can interfere with the desired emission from the thermographic phosphor. In addition, the introduction of impurities, such as lubricant oils, by external means can strongly affect the performance of certain thermographic phosphors, as described in **paper V**. A study by Tabei et al. reported on the quenching of ZnS:(Cu, Al) phosphors by iron-group ions [19]. $Mn^{2+}$, $Ni^{2+}$, $Co^{2+}$, and $Fe^{2+}$ were found to effectively quench the green luminescence of ZnS:(Cu, Al) phosphors through resonant energy transfer processes.

#### *4.1.2.4 Pressure*

In addition to phosphors being thermographic, some phosphors also display a sensitivity of their characteristic luminescence to pressure. Pressure affects both the quantum efficiency and the decay time of the phosphor. Applying pressure results in strain in the thermographic phosphor, which in turn alters the chemical bonds lengths and the atomic configuration. The application of pressure results in a shifting of the spectral distribution as well as alteration of the decay time that is obtained. These alterations are specific for the thermographic phosphor subjected to pressure, the resultant changes in luminescence differ from one phosphor to another. Allison et al. provided a comprehensive survey of thermographic phosphors known to display sensitivity to pressure [1]. Although the phosphors listed there exhibit a sensitivity to pressure, the pressure needed to obtain a significant change in the phosphor luminescence was found to be in the GPa range. These pressure levels are very high compared with those present in combustion engines, its thus being safe to assume that the effects at the pressure levels in combustion engines are negligible.

## 4.2 Remote Temperature Sensing using Thermographic Phosphors

Extracting information carried within the temperature-sensitive luminescence originating from thermographic phosphor makes zero-D, 1-D, and 2-D temperature-sensing possible. Most thermographic phosphors display one format of temperature sensitivity, their response to temperature change being characteristic for the type of phosphor employed. Some phosphors, however, such as YAG:Dy, ZnO:Zn, $BaMg_2Al_{16}O_{27}$:Eu (BAM), and $Mg_3F_2GeO_4$:Mn allow for the use of both sensing methods for temperature deduction purposes. The decay time method and the spectral ratio method have their respective advantages and disadvantages. Their

implementation, the temperature deduction methodology to be employed, and their limitations will be discussed in this sub-section. The studies reported in the thesis exclusively use the decay time method for temperature determination purposes.

### 4.2.1 Spectral Intensity Ratio Method

The spectroscopic distribution of some thermographic phosphors varies with the change in temperature that the phosphor experiences. As the spectroscopic distribution changes, the relative intensity of some of the emission bands vary in relation to one another. By collecting the emission intensity of each of the two bands by means of a 2-D detector, such as an ICCD camera, the intensity ratio at a specific temperature can be obtained. Through changing the temperature of the phosphor, full temperature calibration of this ratio can be achieved. The principles behind the intensity ratio method are shown in Figure 4.3.

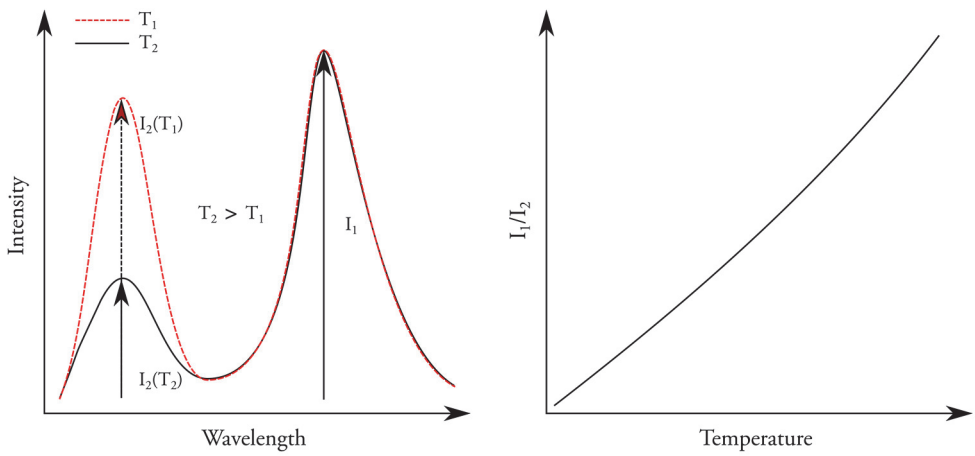


*Figure 4.3 Illustration of use of the spectral intensity ratio method for temperature determination from luminescence originating from thermographic phosphors.*

There are several setup configurations that can be used to determine temperatures by use of the intensity ratio method. The first of these involves use of two cameras, each equipped with an interference filter that transmits one of the bands of the emitted radiation and blocks the others. This configuration requires spatial matching of the two detectors in order to obtain an accurate two-dimensional temperature map. The second configuration utilizes a stereoscope fitted to a single camera which enables the projection of the spectral intensity of each band onto a single detector chip. Stereoscopes can suffer from radiation cross-talk which can jeopardize the accuracy of the temperature determination obtained.

After the acquisition of the intensity images of the two spectral bands that have been selected, the images are subjected to background subtraction and to flat field correction. After which the division of the two intensity maps results in the intensity ratio distribution corresponding to the temperature distribution of the instrumented object. The ratio distribution obtained is then transformed by use of a calibration polynomial to convert the ratios obtained into temperature values.

The spectral ratio method is capable of providing temperature information regarding surfaces with a high degree of spatial resolution. The accuracy and precision of this method is considered to be less than that of the decay time method due to the difference between the intensity ratio and the decay time parameters in terms of the magnitude of temperature sensitivity. Thermographic phosphors decay times usually exhibit a change of 2-3 orders of magnitude as function of a few hundred degrees of change in temperature. In comparison, the intensity ratio typically displays a change of only one order of magnitude for the same degree of temperature change.

The intensity ratio method is susceptible to detector-induced non-linearities that can severely bias the object temperatures obtained [20]. It has also been shown that the intensity ratio method is sensitive to the positioning of the detector that can result in about a 25 K temperature bias [21]. This indicates the necessity of in-situ calibrations so as to minimize the error induced by difference in the position of the detector between calibration and experimentation.

### 4.2.2 Decay Time Method

Unlike the intensity ratio method, the decay time method utilizes the temperature sensitivity of the characteristic decay time of thermographic phosphors to deduce the temperature of objects that are instrumented. The principle of temperature determination by use of the decay time method is shown in Figure 4.4. The decay time of the emitted phosphorescence becomes shorter with an increase in the temperature the phosphor is subjected to. Conducting a temperature calibration of the decay time enables the temperature sensitivity range of a thermographic phosphor to be determined. Most thermographic phosphors have a quenching temperature above which the decay time shows an increased sensitivity to temperature. Each thermographic phosphor has its own individual temperature sensitivity range and quenching temperature. Different emission lines originating from the same thermographic phosphor can display different decay times and different ranges of temperature sensitivity, such as in the case of $La_2O_2S$:Eu phosphor. YAG:Dy, on the other hand, displays similar decay times and ranges of temperature sensitivity for each of the emission bands located around 450, 485, and 585 nm.

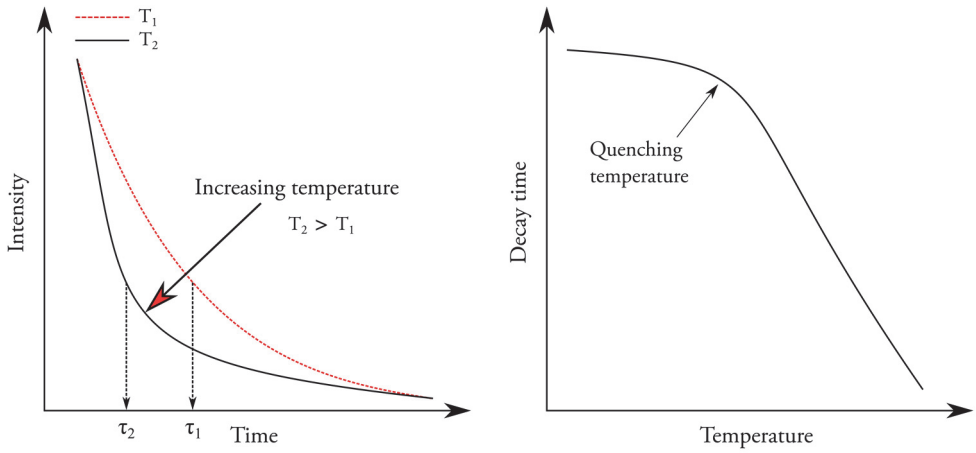


*Figure 4.4 An illustration of the working principle of temperature determination in the decay time method for luminescence originating from thermographic phosphors.*

Both point detectors and 2-D detectors can be employed for capturing the decay time of thermographic phosphors. Point detectors, such as photomultiplier tubes (PMT), microchannel-plate PMTs, photodiodes, and avalanche photodiodes, for examples can retrieve the decay time from an illuminated phosphor-coated surface. Point detectors provide zero-dimensional temperature information. An array of point detectors can be employed for increasing the dimensionality of the measurements to one-dimensional or even to two-dimensional measurements. Two-dimensional detectors, such as ICCD and CMOS cameras, have also been used to capture the decay time of thermographic phosphors and to produce a two-dimensional temperature map of the instrumented surface. Two-dimensional detectors have an advantage by adding extra dimensionality to the temperature information obtained, but their use is severely limited by the low signal levels usually obtained due to the thermal quenching that occurs at high temperatures. On the other hand, the intrinsic high gain of some point detectors (such as PMTs) can provide precise temperature information even at the low emission intensities present at high temperatures. In addition, 2-D detectors require a higher degree of optical access to the environments that are instrumented whereas point detectors can take advantage of optical fibers for capturing the emitted luminescence from the instrumented environments with minimum optical access requirements. The decision to choose a particular detector type is governed to a considerable by such factors as the optical access which is available, the signal strength, and spatial and temporal resolution that is needed.

Detectors convert the decaying luminescence into a decay waveform that is registered by an oscilloscope or by some other type of analog-to-digital conversion device. The decay waveform is then fitted to an exponential function through use of a nonlinear-least-squares solver to calculate the corresponding decay time of the

waveform. The calculated decay time is then translated into a temperature value by using the calibration polynomial obtained earlier.

The decay time method is more precise and accurate than the intensity ratio method is. The decay time method is insensitive to variations in the positioning of the detector, in contrast to the intensity ratio method. With use of high-gain detector, the decay time method is able to measure higher temperatures than the intensity ratio method can. The higher temperature sensitivity of the decay time gives the decay time method a higher degree of precision and sensitivity than the ratio method has. The higher degree of sensitivity also aids in reducing the magnitude of the error that the decay time calculations produce in evaluating the temperatures involved.

#### *4.2.2.1 Possible Sources of Error*

- Detector-induced distortions due to detector saturation can results in a biasing of the temperature results obtained. Detectors operating in a saturation mode can severely distort the generated waveform leading to false decay time and consequently to false temperature. This phenomenon was studied in **papers III** and **IV**.
- Calibration errors due to a malfunctioning thermocouple, or to poor thermocouple-substrate contact, for example, can lead to tens of degrees of error in the temperature that is calibrated. Errors of this type can be propagated to the temperature evaluation without being detected.
- High levels of laser flux can alter the waveform of the decay that is detected. Also, subjecting the phosphor to a wide range of laser fluxes can result in a large temperature error. It is important to note that not all thermographic phosphors display a sensitivity of their decay time to the laser radiation flux that is employed.
- Applying thermographic phosphors in a thick layer can be very intrusive. Thick phosphor layers can perturb the thermal properties of an object that is probed and create thermal gradients through the thickness of the deposited layer. Having thin layers, around 20 μm in thickness, are advisable for negligible intrusiveness [22].
- Some thermographic phosphors display multi-exponential decay waveforms. Fitting a single-exponential function to a multi-exponential waveform is difficult, the calculated decay time strongly dependent upon the fitting parameters that are employed. Caution is called for in fitting multi-exponential decay waveforms, since fitting error can easily lead to error in the determined temperature.
- Substances present in the experimented environment can affect the decay time of a thermographic phosphor. Engine lubricants for example have

been shown to markedly quench the decay time of various thermographic phosphor (**paper V**).

- Interfering luminescence originating either from the experimental environment or from impurities can affect the decay time and lead to erroneous temperatures.
- Other phosphors show a drift in their luminescence intensity and their decay time when subjected to thermal cycling or to temperatures higher than a certain threshold. The thermographic phosphor BAM displays an irreversible degradation in its luminescence and decay time when subjected to high temperatures. The degradation mechanism has been attributed to the europium ions changing from a divalent ($Eu^{2+}$) to a trivalent state ($Eu^{3+}$) [23-26].

## 4.3 Summary of Studied thermographic phosphors

This section provides a summary of the thermographic phosphors studied in the course of the thesis work.

### 4.3.1 $BaMg_2Al_{16}O_{27}$:Eu (BAM)

BAM is a high-quantum-efficiency blue-emitting phosphor usually used for plasma display panels. BAM can effectively excited by 355 nm radiation from an Nd:YAG laser. After excitation, a broadband emission spectrum is observed with band center around 460 nm; see Figure 4.5. The emission at around 450 nm has a decay time that shows sensitivity for temperatures extending over 600 to 1070 K. It is important to note that BAM suffers from degradation in its luminescence and alteration of its decay time when subjected to high temperatures. The degradation mechanism has been credited to changes of in the europium from the divalent state to the trivalent state [23-26]. We have observed a strong effect of heat treatment on the decay time behavior of BAM. In addition, heat treatment does not appear to stabilize the decay time behavior as function of temperature. After each heat treatment, new decay time values were observed for the temperature sensitivity range that was tested.

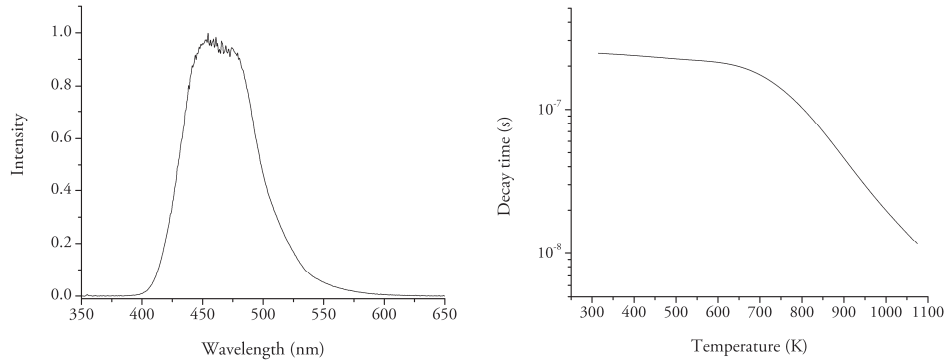


*Figure 4.5 The emission spectrum of $BaMg_2Al_{16}O_{27}$:Eu under 355 nm excitation radiation with the decay time temperature calibration using an interference filter centered at 450 ± 20 nm.*

### 4.3.2 $CdWO_4$

$CdWO_4$ is a thermographic phosphor widely used as a scintillator. $CdWO_4$ has a broadband emission centered at 460 nm when it is excited by 266 nm radiation; see Figure 4.6. The decay time displays a strong sensitivity to temperatures ranging from 293 K up to 570 K. The decay time changes by three orders of magnitude within the temperature sensitivity range of $CdWO_4$. The decay time of $CdWO_4$ was found to be sensitive to the fluence of the excitation radiation, as reported on in **paper IV**. Increasing the laser fluence from 15 µJ to 6 mJ was found to decrease the decay time by 37% as compared with the decay time at the lowest fluence corresponding to an estimated temperature alteration in the range of 15-45 K depending upon the temperature (see Figure 5.19).

### 4.3.3 DySZ

Dysprosium-stabilized zirconia is a conventional thermal barrier material used to shield a variety of engine components from extreme heat loads. The presence of dysprosium makes the compound in question act as a thermographic phosphor showing a characteristic dysprosium emission after 355 nm excitation radiation; see Figure 4.7. The emission band located at around 585 nm displays the strongest intensity. Utilizing this band for phosphor thermometry can make the measurement susceptible to flame luminosity. DySZ has a decay time sensitivity over temperatures extending over 900 to 1200 K. Since both bands, located at 485 and 585 nm, exhibit the same decay time profile as a function of the temperature, it is advantageous to utilize

the 485 nm band for environments contaminated by high flame luminosity. DySZ has a band at 460 nm that becomes visible at high temperature due to thermal activation. The Intensity ratio of the 460 nm to 485 nm band can also be utilized for the intensity ratio method of thermometry.

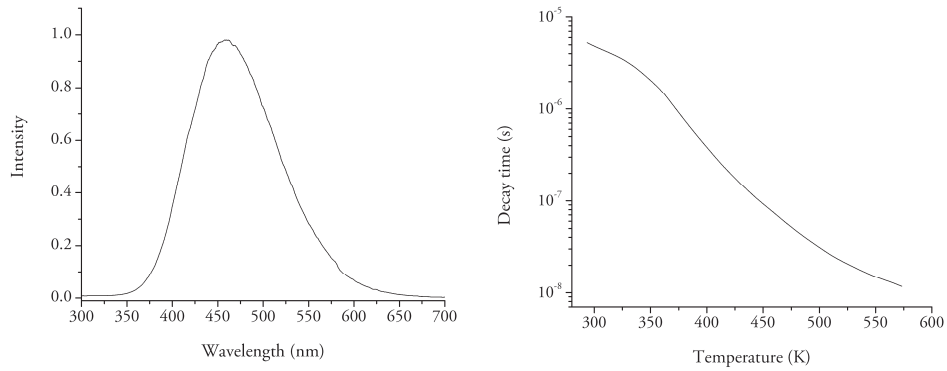


*Figure 4.6 An emission spectrum of $CdWO_4$ when subjected to 266 nm excitation radiation with the decay time temperature calibration being obtained using an interference filter centered at 450 ± 20 nm.*

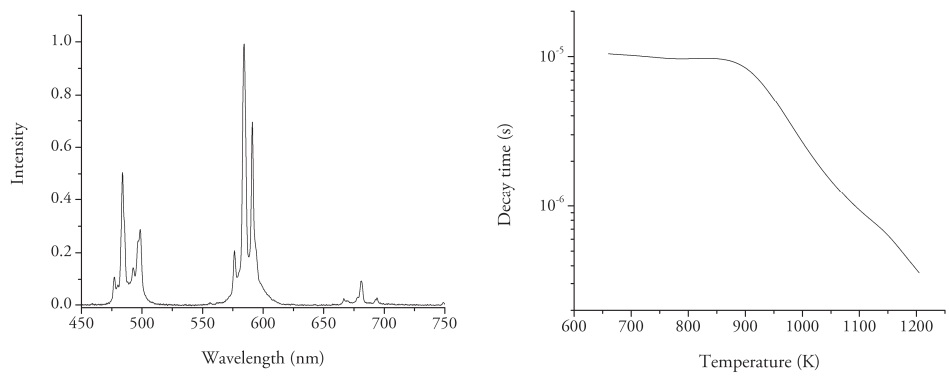


*Figure 4.7 An emission spectrum of DySZ under 355 nm excitation radiation with the decay time temperature calibration being obtained using an interference filter centered at 586 ± 10 nm.*

### 4.3.4 $Gd_2O_2S$:Eu

$Gd_2O_2S$:Eu is a thermographic phosphor that can be excited using 355 nm and 532 nm radiation alike. The possibility of using 532 nm excitation radiation can be beneficial when performing temperature measurements through UV-opaque materials. The emission spectrum of $Gd_2O_2S$:Eu is composed of sharp lines with an intense band located at 625 nm (Figure 4.8). The emission spectra of $Gd_2O_2S$:Eu, when 355 nm and 532 nm excitation radiation is employed, are quite similar with minor differences in the relative intensity of some of the emission lines. The emission peaks located at 538 nm and 555 nm are only visible when 355 nm excitation radiation is used. Figure 4.8 also features the decay time calibration of $Gd_2O_2S$:Eu luminescence after excitation by 532 nm radiation from an Nd:YAG laser. $Gd_2O_2S$:Eu displays a temperature sensitivity extending from 293 K up to 800 K.

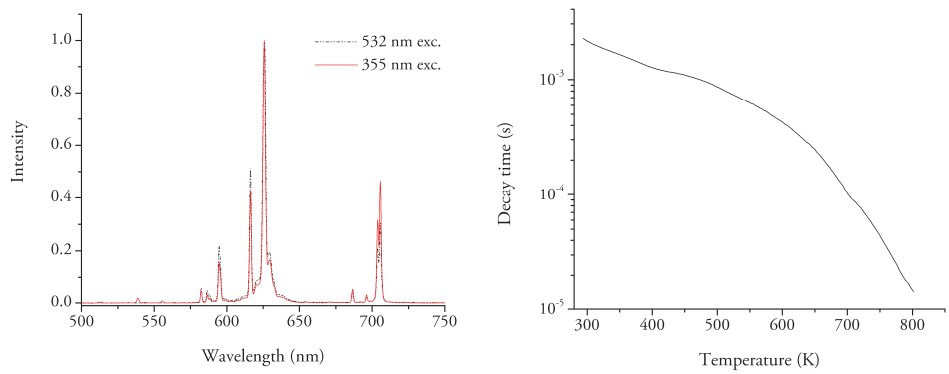


*Figure 4.8 An emission spectrum of $Gd_2O_2S$:Eu at 355 nm and 532 nm excitation radiation with the decay time temperature calibration after 532 nm excitation being obtained using an interference filter centered at 607 ± 18 nm.*

### 4.3.5 $La_2O_2S$:Eu

$La_2O_2S$:Eu has an emission spectrum that is also characterized by sharp emission lines. The emission lines located at 512, 538, and 624 nm are usually employed for decay time phosphor thermometry (Figure 4.9). Each of these emission lines has a different decay time sensitivity to temperature and can be used interchangeably to extend the total temperature sensitivity range of $La_2O_2S$:Eu phosphor. The decay time sensitivity of the 538 nm emission line is presented in Figure 4.9. This emission line exhibits a decay time that has a sensitivity extending from 350 K up to 625 K. The 512 nm emission line has a temperature sensitivity starting from lower temperatures

while the 624 nm emission line sensitivity starts at a higher temperature compared to the 538 nm emission line.

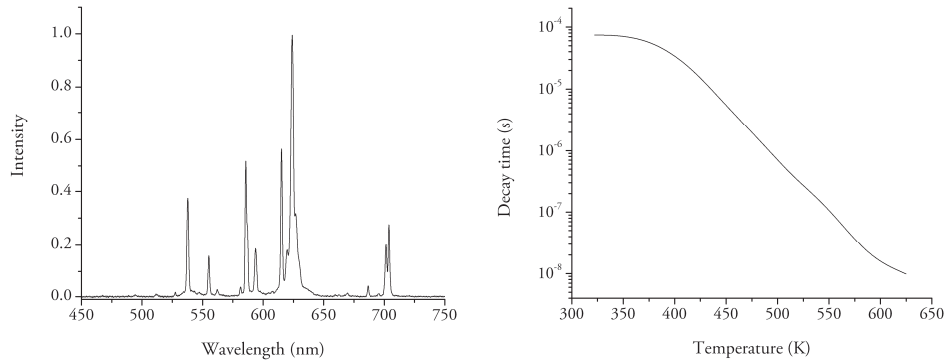


*Figure 4.9 An emission spectrum of $La_2O_2S$:Eu at 355 nm excitation radiation with the decay time temperature calibration using an interference filter centered at 540 ± 5 nm.*

### 4.3.6 $Mg_3F_2GeO_4$:Mn

$Mg_3F_2GeO_4$:Mn is a thermographic phosphor that has the capability of temperature sensing using both the intensity ratio and the decay time method. The intensity ratio of the emission peaks at 631 nm and 656 nm is temperature-sensitive. $Mg_3F_2GeO_4$:Mn can be effectively excited with 266 nm and 355 nm radiation generated by an Nd:YAG laser. Figure 4.10 represents the corresponding emission spectrum obtained after excitation by 355 nm radiation. The decay time of the emission line at 656 nm is also presented. $Mg_3F_2GeO_4$:Mn displays a temperature sensitivity extending from 293 K up to 1070 K. The decay time displays a greater sensitivity for temperatures higher than 670 K.

### 4.3.7 $Y_2O_3$:Eu

$Y_2O_3$:Eu, like $Gd_2O_2S$:Eu phosphor, can be effectively excited using both 355 nm and 532 nm radiation from an Nd:YAG laser. The emission spectrum, with 532 nm excitation, is characterized by an intense peak at 611 nm (Figure 4.11). The decay time of the 611 nm emission line has a multi-exponential profile with an intense rapidly decaying component and a weak slowly decaying component. Due to the ability of $Y_2O_3$:Eu phosphor to be excited by 532 nm radiation, it has the capability to act as a sub-surface temperature sensor for UV-opaque plasma sprayed thermal barrier coatings,

as described in **paper VII** and by Eldridge et al. [27]. The decay time originating from the 611 nm luminescence is sensitive to temperatures extending over 670-1030 K.

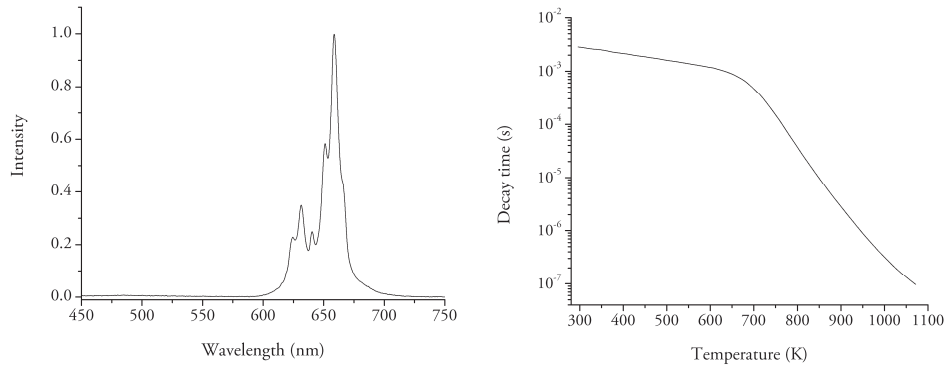


*Figure 4.10 An emission spectrum of $Mg_3F_2GeO_4$:Mn under 355 nm excitation radiation with the decay time temperature calibration being obtained using an interference filter centered at 656 ± 5 nm.*

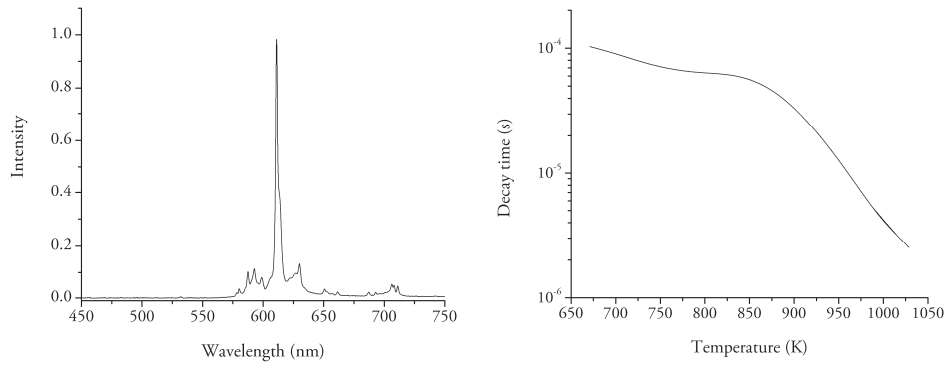


*Figure 4.11 An emission spectrum of $Y_2O_3$:Eu exposed to 532 nm excitation radiation with the decay time temperature calibration using an interference filter centered at 607 ± 18 nm.*

### 4.3.8 ZnO:Zn

ZnO:Zn is a phosphor widely used in LED displays and scintillators. It displays a strong spectral shift as the temperature of the phosphor changes. ZnO:Zn has two main

emission bands at 390 nm and 510 nm (Figure 4.12). The intensity ratio of the two bands displays a strong sensitivity to temperature.

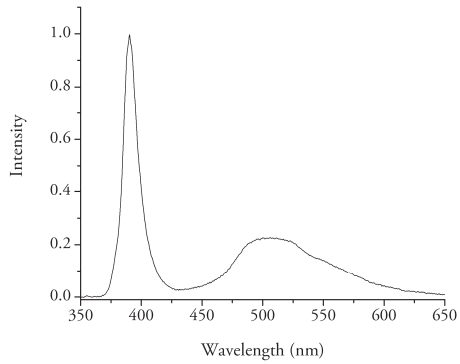


*Figure 4.12 An emission spectrum of ZnO:Zn at an excitation radiation of 355 nm.*

### 4.3.9 ZnS:Ag

ZnS:Ag is a blue-emitting phosphor showing a high quantum efficiency. Upon excitation by 355 nm laser radiation, ZnS:Ag emits a broadband spectrum with a band center at 450 nm, as shown in Figure 4.13. Between 293 K and 400 K, the decay time becomes slower with increasing temperature. At temperatures higher than 400 K, ZnS:Ag display a monotonic change in its decay time with increasing temperature. ZnS:Ag is sensitive to temperatures between 400 K and 875 K. The decay waveform of ZnS:Ag resembles a double-exponential profile.

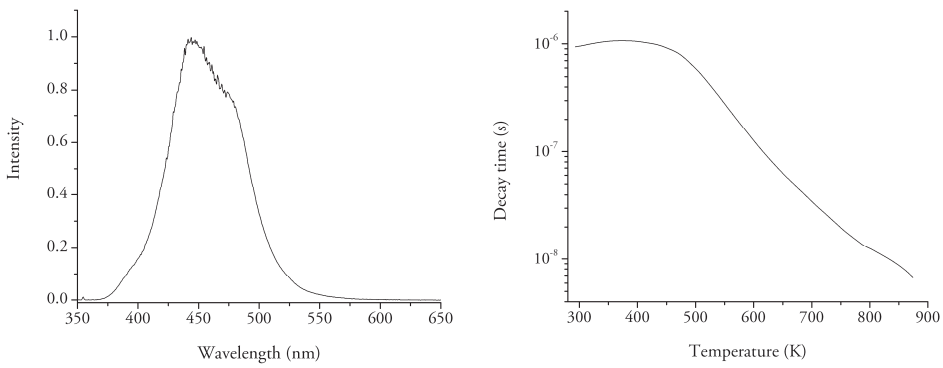


*Figure 4.13 An emission spectrum of ZnS:Ag under 355 nm excitation radiation with the decay time temperature calibration using an interference filter centered at 450 ± 20 nm.*

## 4.4 Phosphor Selection

The selection criteria for thermographic phosphors in a given application are strictly governed by both the conditions present in the experimental environment and the requirements imposed on the temperature information attained. The range of temperatures the instrumented object is exposed to is a major criterion here, since each thermographic phosphor has a predetermined operational range of temperatures, as shown in Figure 4.14.

The temporal resolution required is another limiting factor in the selection process for thermographic phosphors that show a decay time temperature sensitivity. Internal combustion engines, such as spark ignition engines, operate at high speeds, reaching several thousand rotations per minute (rpm). In order to achieve, for example, a single crank angle degree of resolution for an engine operating at 1200 rpm, the decay time of the thermographic phosphor needs be shorted than 50 μs.

In diesel engines, Soot luminosity can severely distort the observed decay waveform to a point at which measurements are no longer viable. Thus, thermographic phosphors having emission lines that are close to the blue end of the electromagnetic spectrum are to be preferred in environments in which soot luminosity is an issue.

Under other circumstances, it is not possible to use UV-radiation to excite thermographic phosphor, thus limiting the thermographic phosphors that can be potentially employed to only a few phosphors that can be effectively excited by visible radiation.

In other applications, phosphors having a high quantum efficiency are needed to overcome the luminescence emitted by the experimental environment. Strong emission intensity allow for the differentiation of luminescence generated by the applied thermographic phosphor from the background luminescence. Implementing spectral and temporal filtering helps suppress the background radiation, thus improving the signal-to-noise ratio and consequently the temperature precision involved.

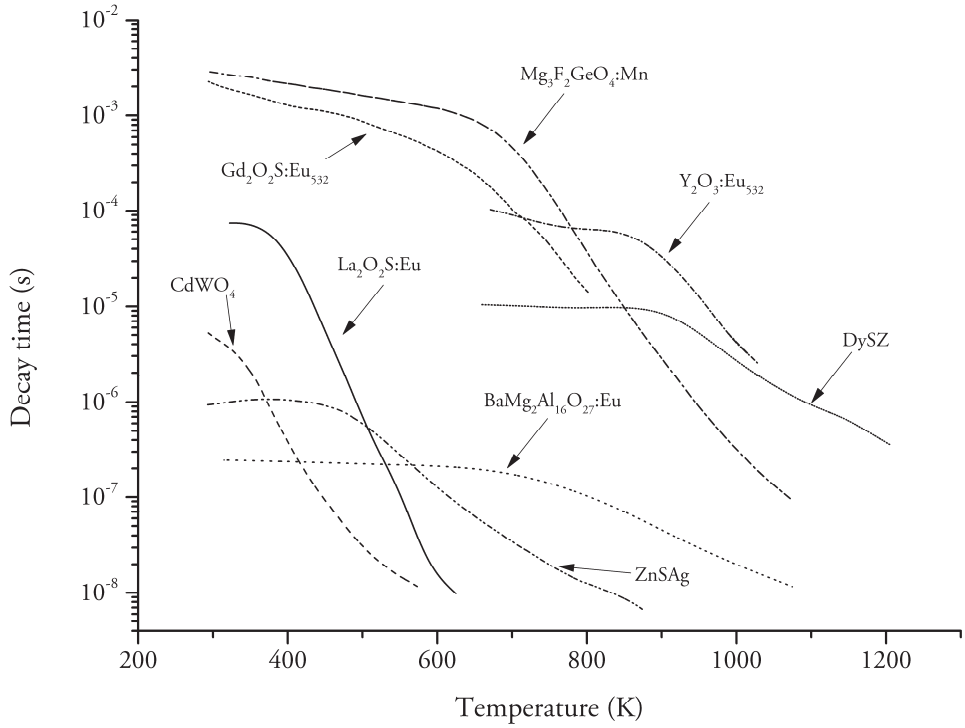


*Figure 4.14 Decay time calibrations of thermographic phosphors studied in the thesis work.*

## 4.5 Decay Time-based Phosphor Thermometry Experimental Setup

The application of decay time based phosphor thermometry to a target object requires an experimental setup composed primarily of a pulsed laser, a phosphor coating applied to the target surface, collection optics, a detector, and a data acquisition system. Figure 4.15 presents a sketch of a typical experimental setup used to perform decay time based phosphor thermometry. A pulsed laser, usually producing laser radiation in the UV part of the electromagnetic spectrum, was used to excite a thin layer of a selected thermographic phosphor that has been coated onto the surface of the target object. The laser beam was directed towards the target by means of dichroic mirrors that served to reflect the laser radiation. After excitation by the incident radiation, luminescence was emitted by the thermographic phosphor and was collected by collection optics. The collection optics were usually composed of a number of lenses that concentrated the radiation that was collected onto the detector input window. One or more interference

filters were placed in front of the detector so as to spectrally select the desired portion of the luminescence and to suppress any spurious radiation. The detector then converted the input luminescence signal into an electric output signal that was read by a data acquisition system. The decay waveforms that were acquired were then saved for later post processing and temperature determination.

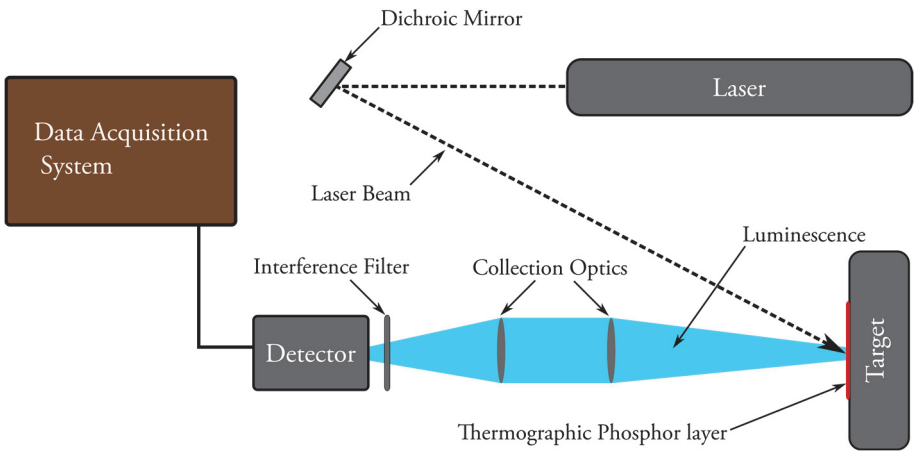


*Figure 4.15 Sketch of a typical experimental setup used for decay time phosphor thermometry.*

# 5 Development of Phosphor Thermometry Technique

This section provides a summary of the work carried out as an effort to develop the decay time-based phosphor thermometry technique. The work involved aimed at optimizing in so far as possible the precision of the technique as well as providing insight into covert sources of error that could introduce biases in the temperature assessments arrived at. Improvements in the established thermographic phosphor calibration versus temperature reflect directly as an improvement in the accuracy of the temperatures obtained. Detector-induced biases can severely reduce the quality of the determined temperatures and render the information obtained useless or nearly so. It is also important to consider the effects that the environment and the co-existing materials can have on the performance of this technique. This chapter presents a summary of the findings and developments obtained aimed at the optimization of the decay time-based phosphor thermometry technique. The chapter covers the material published in **papers I** through **V**.

## 5.1 Automatic Calibration

Calibration of the decay time of the thermographic phosphor is needed to convert the measured decay time into temperature values. This calibration function is usually based on measuring the decay time at predetermined temperatures, the calibration polynomial being constructed by interpolating between the calibration points obtained. Ceramic ovens are usually used to heat up a sample of the thermographic phosphor in question coated onto a metallic substrate to be calibrated. Thermocouples are used to monitor the oven temperature and assuming thermal equilibrium, the measured oven temperature is presumed to be equal to the temperature of the thermographic phosphor sample. Thermal equilibrium requires prolonged duration of time to be established, which could significantly increase the time required to obtain a single calibration. The sample temperature could deviate from the oven temperature, leading to errors in the established calibration. Radiation losses from the sample could also lead to biases in the calibration. Thus, a robust and reliable calibration procedure would serve to ensure

that the calibration is accurate and should result in an improvement in the achieved temperature accuracy.

The conventional calibration (point-by-point calibration) described above suffers from long calibration duration and plausible inaccuracy due to possible deviations between the temperature of the thermographic phosphor sample and that of the thermocouple. The need for a reliable calibration procedure motivated the design and implementation of a continuous and automatic calibration procedure capable of achieving a calibration with an accuracy of ± 1.5 K up to ± 4 K, depending upon the range of calibration temperatures involved. The ability to acquire the calibration continuously resulted in a reduction by a factor of 4 in the time needed to achieve complete calibration as compared with the duration needed by the conventional procedure.

The calibration routine developed was composed of two separate elements, one being the hardware and the other the software. Both elements were designed and implemented with maximum accuracy in mind. The hardware element included the design of a new calibration substrate over which the calibrated phosphor is sprayed. The substrate design incorporated an embedded thermocouple system for minimizing the thermal gradients across the various dimensions of the substrate. The software element, on the other hand, was composed of a hardware-control software that synchronized the different hardware elements. In addition, the software included a preprocessing software that simultaneously acquired the phosphorescence decay curve and the thermocouple temperature and saved these on a single file for later post-processing. The developed calibration routine was reported on in **papers I** and **II**.

### 5.1.1 Hardware

This section describes the design chosen for the substrate and the corresponding thermal analysis carried out using a heat transfer simulation. The heat transfer study was performed to assess the magnitude of the thermal gradients due to the continuous ramping of the substrate temperature.

#### *5.1.1.1 Substrate Design*

The substrate was designed in a disk shape that had a diameter of 41 mm and a thickness of 6 mm. Hastelloy-C alloy, a corrosion-resistant alloy having low thermal expansion coefficient, was selected as an appropriate material for the substrate. The corrosion resistance maintains the surface quality of the substrate after numerous calibrations, which in turn is optimal for the adherence of the coated thermographic phosphor. The low thermal expansion coefficient is suitable for preventing flaking of the coated layer, due to the difference in the rate of expansion of the two materials. Hastelloy-C alloy has a high melting temperature (1550 K) making calibrations of up

to 1500 K feasible with use of this substrate. Placing the calibration substrate in the center of the oven results in an even thermal power distribution at the boundaries of the substrate. Four type-K (class 1) thermocouples were embedded and press-fitted within the substrate at a depth of 5 mm. This placement ensures maximum contact with the substrate and minimizes the temperature gradient between the surface of the substrate and the thermocouple contact. The thermocouples employed were placed in an Inconel-600 sheath, 2 mm in diameter, for increased robustness and the sheath also served as a substrate holder when placed inside the calibration oven. Two thermocouple distributions, one of them tight (4 mm off-center) and the other wide (15 mm off-center), were selected for assessing the possibility of the existence of thermal gradients across the substrate. A schematic design of the substrates is shown in Figure 5.1.

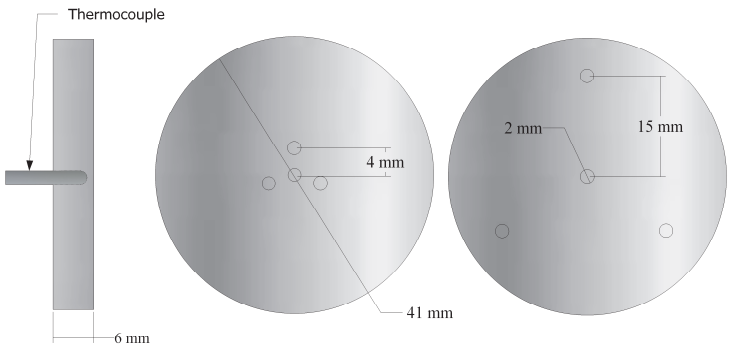


*Figure 5.1 Schematic of the design of the calibration substrate with its embedded type-K thermocouples.*

### *5.1.1.2 Heat-transfer study*

Thermal gradients can develop within the substrate due to the continuous ramping of the temperature. Thermal gradients between the surface on which the phosphor is coated and the site of the thermocouple contact can lead to errors in the calibrated temperature and eventually in the determined object temperature. The two different thermocouple distributions described earlier provide insight into the thermal gradients in the radial position caused by the uneven heating by the oven. They fail, however, to provide insight into the gradients that may possibly be present between the surface of the substrate and the locations within the substrate at which the thermocouples are embedded.

Using heat-transfer modeling tool provided by COMSOL Multiphysics Software, enabled a detailed study of the thermal gradients as a function of the heating rate of the calibration oven. COMSOL utilizes the finite element method to solve the conductive heat transfer equation (Equation 5.1) throughout the simulated substrate geometry.

$$\rho C_p \frac{\partial T}{\partial t} - \nabla.(k\nabla T) = Q \qquad \text{Equation 5.1}$$

Where ρ is the density (kg.m$^{-3}$), $C_p$ is the specific heat capacity at constant pressure (J.kg$^{-1}$.K$^{-1}$), T is the absolute temperature (K), k is the thermal conductivity (W. m$^{-1}$.K$^{-1}$), and Q is the amount of heat (W. m$^{-3}$). The thermal coefficients (ρ, $C_p$, and k) of the Hastelloy C-4 substrate material were plugged in from the library of material properties available within the COMSOL software. Setting the heat flux, q, to 600 W. m$^{-2}$ creates a heating rate that matches that attained by the calibration oven at 4 K.min$^{-1}$. The initial temperature of the substrate model was set to 293.15 K. The solver provided a solution as a function of time so as to assess the growth of thermal gradients as the oven temperature increases over time.

For the model to be considered valid, a number of assumptions need to be made. The first assumption is that only conductive heat transfer can be considered significant within the substrate boundaries, whereas the net radiative and convective heat losses are considered insignificant. During the actual calibrations, the oven ports are sealed either by quartz windows or by a thermal insulator so as to drastically reduce the heat loss due to convection to the surrounding environment. The second assumption is that uniform heating is delivered to all of the surfaces of the substrate. In real life, this can best be achieved by suspending the substrate in the center of the heating tube of the oven. All of these assumptions were validated by a separate heat transfer model that took into consideration the geometry of the entire oven.

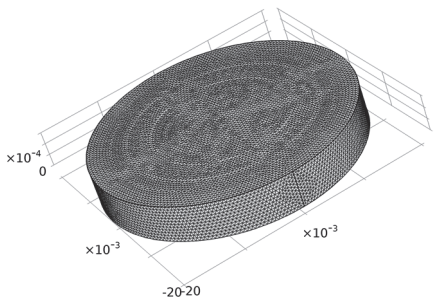


*Figure 5.2 Substrate model created in COMSOL software with the corresponding mesh applied to the geometry.*

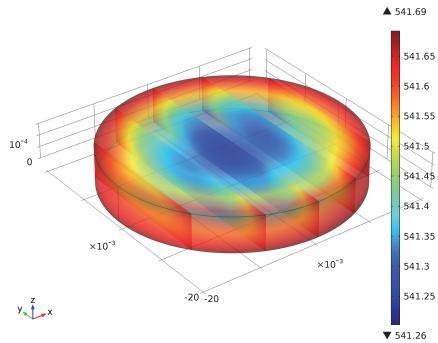


*Figure 5.3 Three-dimensional temperature distribution in kelvin (K) of the Hastelloy substrate at t = 3600 sec.*

The substrate geometry was modeled in COMSOL and a mesh was applied for dividing the model geometry into smaller volumes. For each volume, the solver solves the conductive heat transfer function as function of time. A schematic of the mesh in the substrate model geometry is shown in Figure 5.2. The final mesh divided the model volume into 961,000 separate elements.

COMSOL program solved the heat transfer problem for the entire volume as function of time for a period of 3600 seconds. The results are a three-dimensional map of temperature that evolves as function of time. A snapshot of the temperature map at t = 3600 seconds is shown in Figure 5.3. The results validate the concept that the thermal gradients extending through the substrate being negligible. Both radially and through the thickness of the model, the maximum temperature gradient is less than one Kelvin as shown in Figure 5.4 and Figure 5.5. The results shown in Figure 5.4 represent the development of the temperature as a function of time (for a period of 3600 seconds) at several depths from the surface of the radial center. Whereas Figure 5.5 depicts the radial temperature distribution at time t = 3600 seconds. The results indicate that the thermal gradients within the designed calibration substrate to be negligible for heating rates of up to 4 $K.min^{-1}$.

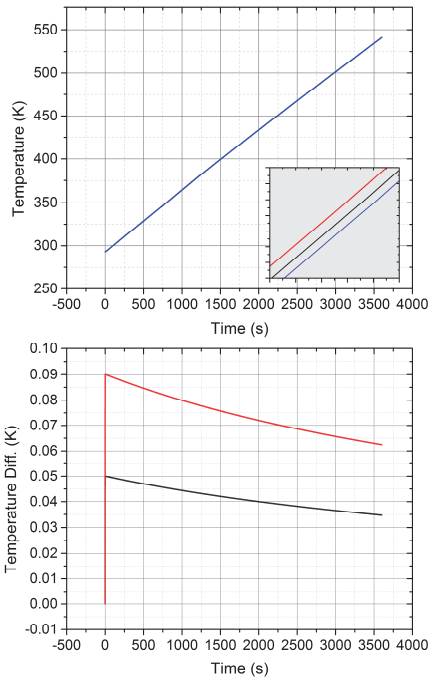


*Figure 5.4 (Top) The temperature history at the radial center of the substrate at a 0 mm depth (red), a 1 mm depth (black), and a 3 mm depth (blue). The inset presents a zoom of the temperature history. (Bottom) represents the difference in temperatures at the surface and at 1 mm depth (black) and at the surface and at a 3 mm depth (red).*

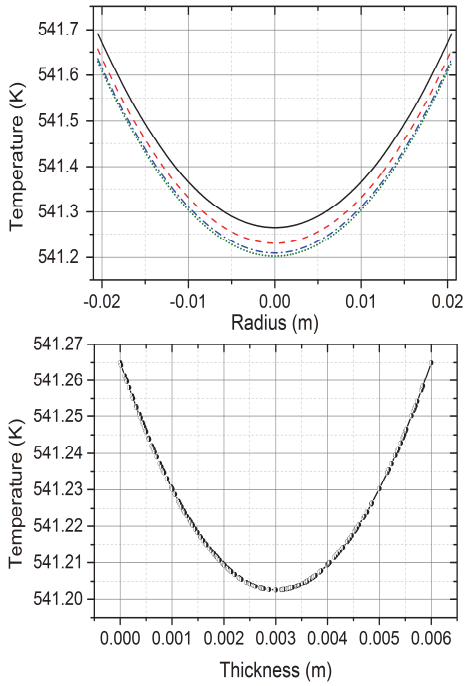


*Figure 5.5 (Top) The temperature profile at t = 3600 s shown as a function of the substrate disk radius at the surface (solid black line), at a1 mm depth (dashed red line), at a 2 mm depth (dash-dotted blue line), and at a 3 mm depth (double dotted-dashed green line). (Bottom) The temperature profile at t = 3600 s as a function of depth.*

### 5.1.2 Software

Hardware control, data-acquisition synchronization, waveform pre-processing, and data saving are all tasks that are handled by the automatic calibration software employed, which is written in LabVIEW programming language. The software enables for continuous and automatic calibration process, which reduces the time duration needed to complete a given calibration. In addition, optimal acquisition synchronization between the thermocouples recording of the substrate temperature and of the acquired decay waveform is provided. Execution of the automatic calibration

routine occurs in several stages. Once all the elements of the execution cycle have been completed, the process is repeated until the program is terminated.

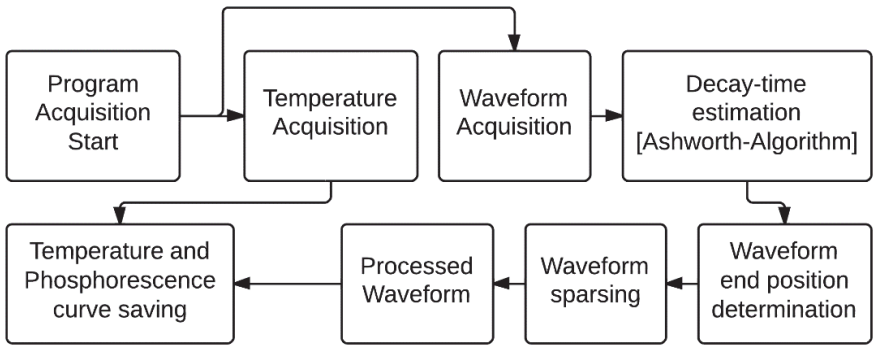


*Figure 5.6 A schematic of the order of execution of the individual processes in the automatic calibration routine.*

The routine is operated continuously while the calibration oven is set to a constant heating rate less than or equal to 4 $K.min^{-1}$. At the beginning of every acquisition cycle of the routine, the acquisition of the temperature and that of the decay waveform are synchronized. The individual temperatures from each of the four thermocouples are averaged. Afterwards, the registered waveform is pre-processed so as to facilitate the later decay-curve-fitting process. The pre-processing includes sparsing and initial evaluation of the decay time of the waveform. After pre-processing, the acquired substrate temperatures, equivalent to the thermographic phosphor temperature, are combined with the respective pre-processed decay waveform. This process is repeated for the duration of the calibration at the desired acquisition rate. A schematic of the individual processes occurring during each of the routine cycles is presented in Figure 5.6. The final result is a calibration composed of several thousand calibration points, which enables for the extraction of an accurate calibration polynomial. The high density of the calibration points permitted the development of a temperature extraction algorithm that does not require the evaluation of the decay time of the waveform [28]. Instead, the algorithm compares the experimental decay waveform to a library of calibration waveforms to obtain the best possible match. The best matched calibration curve determines then the temperatures the thermographic phosphor underwent. This method of temperature determination is highly advantageous, particularly for thermographic phosphors that display multi-exponential decay profiles.

### 5.1.3 Finalized Automatic Calibration

The final calibration experimental setup shown in Figure 5.7 includes the laser, an electrical furnace, the phosphor-coated substrate, a data acquisition unit, Photo-detector (PMT), and a digital oscilloscope. This setup was employed to acquire calibrations using both the conventional method and the automated method for comparison purposes. A comparison calibration of the $Mg_3F_2GeO_4$:Mn thermographic phosphor is shown in Figure 5.8. Figure 5.8 demonstrates that the developed calibration routine delivers an accurate calibration with high density of calibration points for successful temperature determination.

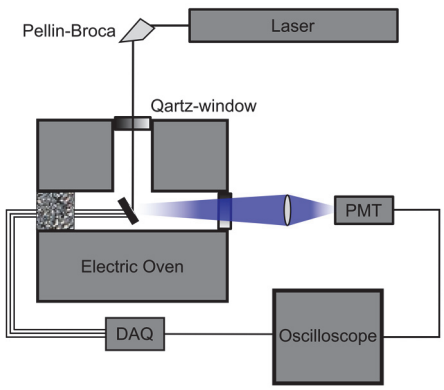


*Figure 5.7 A schematic of the experimental setup of the developed automatic calibration.*

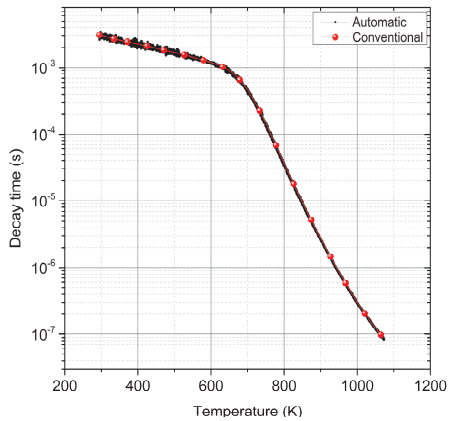


*Figure 5.8 A conventional and an automatic calibration of $Mg_3F_2GeO_4$:Mn thermographic phosphor.*

## 5.2 Detector Response Characterization

To ensure the greatest precision and accuracy possible in temperature determination using phosphor thermometry, all sources of distortion and biasing need to be subjected to scrutiny. Inspecting all possible sources of error enables one to improve the technique employed and in turn obtain trustworthy temperature measurements. In the present section, the investigations reported on in **papers III** and **IV** are described. Detector-induced distortions in the waveform of the decay can have serious negative effects on one's assessment of the temperatures involved and lead to errors tens of kelvins in magnitude [29]. Distortions occurring within the photodetector can also affect the generated phosphorescence waveform. The linearity

of the conversion process carried out by the detector is essential to ensure a true reproduction of the decaying luminescence and thus for accurate temperature retrieval. Detector-induced distortions are often by their nature highly discrete and can easily pass undetected.

In a previous study involving use of the spectral ratio method, the nonlinearity of intensified-CCD cameras in their application to phosphor thermometry was reported [20]. The authors observed that the ICCD camera deviated from linearity when the signal counts exceeded a certain level. The deviation from linearity resulted in an estimated temperature that deviated by 200 K from the true value. The investigations reported in **paper III** dealt with detector-induced distortions in several different point detectors. The tested detectors were photomultiplier tubes (regular and time-gated), a microchannel plate PMT, and an avalanche photodiode. In comparing them, a time-gateable PMT was found to be the most suitable detector, which provided a linear response within a wide range of incident phosphorescence intensities and detector gains. The luminescence provided by $CdWO_4$ was selected for testing the response of all the detectors. $CdWO_4$ provided phosphorescence with decay times that extended from 10 ns at 580 K up to 10 μs at 290 K. This wide range of decay times enabled the effects of the length of the decay time on the behavior of the detectors to be investigated. In **paper IV**, investigation of the effect of the detector response on the temperature assessment was continued. Whereas **paper III** compared different point photodetectors, **paper IV** presented a comparison of four PMTs of identical product type so as to assess unit-to-unit variations. **Paper IV** also addressed other possible sources of error, such as the oscilloscope channel settings and the initially strong luminescence peak present prior to the long decay, a peak that could contribute to the overall inaccuracy in the temperatures measurements obtained.

### 5.2.1 Detector Response Matrix

To investigate the way in which photodetectors can distort the generated output decay signal, a detector response matrix, that characterizes the decay time as a function of the phosphorescence intensity and the applied detector gain was devised. Response matrices for each of five different temperatures were obtained for each of the detectors that were studied. At each pre-set temperature, the furnace temperature was stabilized, then the response matrices were acquired for each of the detectors.

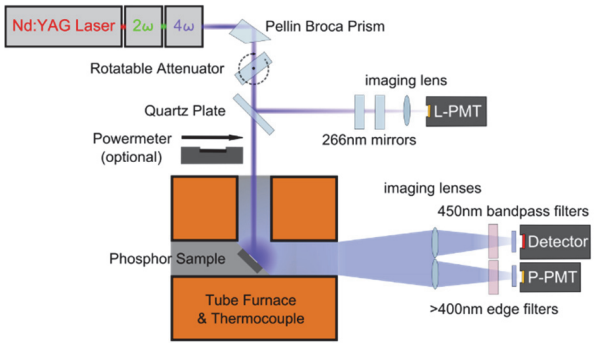


*Figure 5.9 A schematic of the experimental setup used to build the response matrices for each of the detectors.*

| Detector Type | Name |
|---|---|
| $PMT_1$ | H6780-04 |
| $PMT_2$ | H11526-20-NF |
| MCP-PMT | R5916U-50 |
| APD | S5343 |

*Table 5.1 The photodetectors tested.*

To ensure that the different detectors were subjected to phosphorescence of the same levels of intensity, a reference system from two identical PMTs was constructed; see Figure 5.9. The first reference PMT (L-PMT) was calibrated against a laser power meter that provided a measure of the laser energy on shot-to-shot basis. The P-PMT, in turn provided a reference in terms of the intensity of the incident phosphorescence radiation for each of the detectors that were investigated. Later, the read-out signal from the P-PMT was used to sort the response matrices according to the reference phosphorescence intensity, which was later converted to the number of incident photons in 1 ns. To construct a complete response matrix for a given detector at a preselected temperature, a particular electrical gain for the detector was selected and then the phosphorescence intensity was scanned. This provided a single row in the matrix. By changing the electrical gain of the detector to each of the preset levels and repeating the scan, a complete response matrix could be obtained. It is important to bear in mind that, because of the differences between the detectors in the operation mechanisms involved and in the inherent properties of the various detectors, a different set of gains was selected for each of the detectors.

Some of the detectors that were tested were operated in different modes so as to investigate whether the operation mode involved affected the response of the detector. $PMT_1$ was also run with an attached electrical amplifier which resulted in lesser range of gains being utilized than are usually employed in normal operations. $PMT_2$ has the capability of being time-gated and it was operated in both a normal and in a time-gated way to determine whether time-gating away the initial portion of the decay would affect the detector response. The MCP-PMT can only be run in a time-gated mode with a maximum time gate width of 10 μs. Response matrices for each of the detectors and their corresponding operating modes at five different sets of decay times originating from $CdWO_4$ phosphor were acquired. The different decay times were obtained by

raising the temperature of the $CdWO_4$ sample starting at 294 K, and continuing with 373, 454, 519, and 561 K.

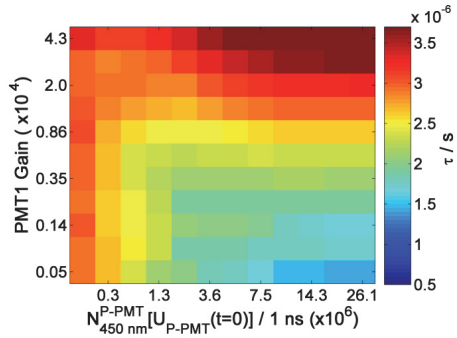


*Figure 5.10 Response matrix of $PMT_1$ at 373 K.*

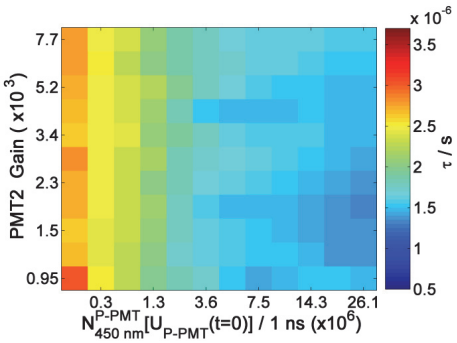


*Figure 5.11 Response matrix of $PMT_2$ at 373 K.*

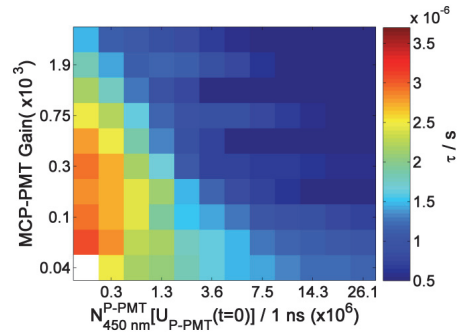


*Figure 5.12 Response matrix of MCP-PMT at 373 K, triggered 10 ns before the signal arrived.*

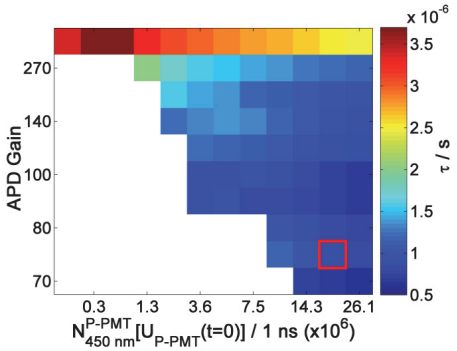


*Figure 5.13 Response matrix of APD at 373 K.*

Figure 5.10, Figure 5.11, Figure 5.12, and Figure 5.13 represent the constructed response matrices as a function of the calculated decay time for each of the four detectors subjected to luminescence originating from $CdWO_4$ at 373 K. In theory, if the detectors display a linear response, the response matrix should show similar decay times across the entire matrix, apart from minor discrepancies due to evaluation errors. Two conclusions can be readily drawn from the figures shown. The first conclusion is that the decay time is strongly affected by the operating conditions of the detector. The other conclusion is that the response of each of the detectors is unique to a particular detector, which suggests that a response matrix is needed in order to adequately

understand the detector effects with respect to the calculated decay time and the later temperature assessment.

The high decay time zone observed at low phosphorescence intensities can be attributed to changes in the decay time $CdWO_4$ due to changes in the laser fluence. Similar effects have been reported for other phosphors [30]. The extent of the detector-induced distortions of the decay time in relation to the temperature can be clearly seen in Figure 5.14. Artificial temperatures were calculated on the basis of a previously obtained phosphor temperature calibration. The temperatures showed a spread of 40 K in temperature, whereas the actual phosphor temperature was held constant at 373 K during acquisition of the response matrix. Temperature distortions of such magnitude are detrimental to phosphor thermometry and can render it useless or, even worse, provide false temperature information.

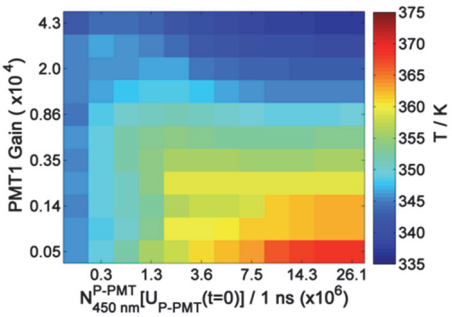


*Figure 5.14 Estimated temperatures as calculated from Figure 5.10 using temperature calibration data of $CdWO_4$. The actual phosphor temperature was kept constant at 373 K.*

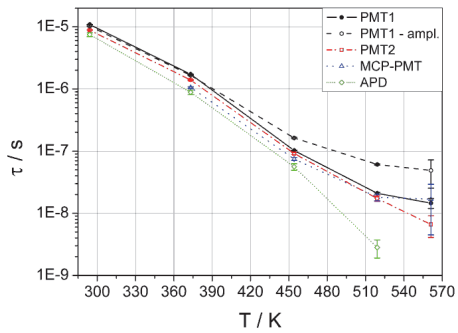


*Figure 5.15 Reconstructed temperature calibration points for all of the detectors, as gathered from a fixed response matrix element. The Error bars indicate values at one standard deviation from the mean value.*

Decay times from a fixed matrix element in the response matrices of all of the detectors were plotted as function of the phosphor temperature so as to obtain a temperature calibration curve (Figure 5.15). Although all of the detectors were subjected to identical conditions, each individual detector provided a unique phosphorescence decay time calibration polynomial.

It is important to note that when $PMT_1$ was operated with an electrical amplifier and with a lower detector gain range, $PMT_1$ showed a better response. The response of the amplifier-$PMT_1$ system resembled that produced by $PMT_2$. On the other hand, operating $PMT_2$ in a time-gated mode was found to have no effect on the response of the PMT, the resultant response matrix is similar to that obtained for a normal operating mode.

Of the various detectors that were tested, the time-gateable PMT ($PMT_2$) exhibited the best performance in terms of linearity as a function of the decay time. The APD, on the other hand, provided the best sensitivity, as can be seen in Figure 5.15. Due to its intrinsic low gain, APD cannot be used under low illumination conditions. The MCP-PMT used has a gate width limit of 10μs, which means that decay times longer than 2-3 μs could not be registered by this detector. The investigations carried out showed the detector to have a significant effect on the performance of the phosphor thermometry technique, thus the characterization of the detector response is essential prior to its use in detecting phosphorescence signals.

### 5.2.2 Detector Response and Laser Energy Dependence

The results reported in section 5.2.1 in which the different detectors were compared indicated the time-gateable PMT to be the most favorable option of the different detectors that were selected. In this section, the results of the investigations carried in **paper IV** are reported on. The detector found to be most favorable, time-gateable PMT ($PMT_2$), was subjected to further experimentation in order to determine the sources of the distortions present in the generated output waveform. The output signal of the detector and the detector gain were used as parameters for characterizing the response of the PMT. Current-output type PMTs have been studied extensively, and most manufacturers set a limit of 100 μA as being the maximum current output of a PMT for a linear response. This upper limit was established, however, for PMTs subjected to a constant illumination over time. In the case of the detection of phosphorescence signals, the signal is usually temporally short (ns to ms time-scale), which can affect the detector in a different manner than if it was subjected to continuous illumination. Several studies have demonstrated a linear PMT response at PMT output currents higher than the previously set limit of 100 μA [31, 32].

As taken up in section 5.2.1, most of the detectors displayed a long decay time at a low incident photons count, this suggesting there to be phosphor-related variations rather than detector-induced distortions involved here. During the present investigation, variations in the laser energy were decoupled from the phosphorescence luminescence intensity variation through holding the laser energy at a constant level while varying the incident phosphorescence intensity by means of an iris placed in front of the PMT. Thus, any variations in the decay times that occurred can be attributed to the detector response instead. $CdWO_4$ was utilized as the luminescent source for this investigation too.

During this test, the maximum value for the voltage output signal was held at two pre-designated levels, 30 and 300 mV, for all of the acquired measurement points. To maintain the output signal at either of the pre-selected levels, the detector gain and incident phosphoresce intensity were varied interchangeably. This means that when a

lower gain was utilized, a higher luminescence intensity was allowed to fall onto the detector window. The phosphorescence intensity was varied either by changing the incident laser fluence upon the phosphor (ranging from 15 μJ to 5 mJ), or by holding the laser fluence constant (at 5 mJ) while changing the diameter of the iris. The detector gain was controlled by the control voltage applied to the PMT. As the control voltage increases, the PMT gain increases too.

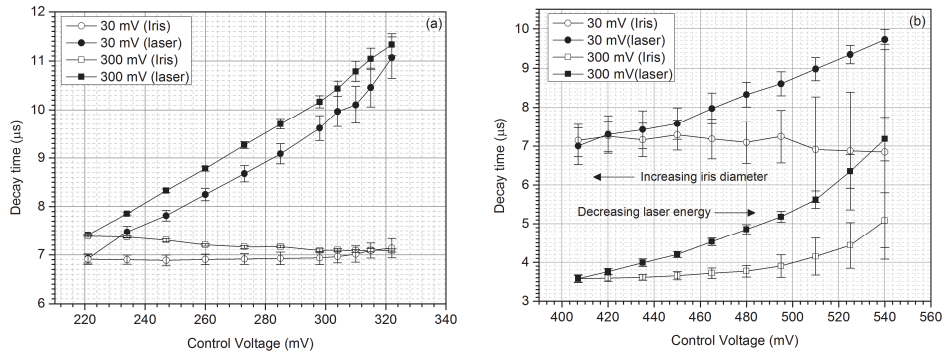


*Figure 5.16 Excitation energy dependence test for $CdWO_4$. The light intensity was varied either by means of the laser energy employed, from 15 μJ to 5 mJ (●/■), or by changing the diameter of the imaging lens while employing a constant laser energy of 5 mJ (○/□). The maximum electrical output signal was kept constant at either 30 mV (●/○) or 300 mV (■/□).*

Two different ranges of control voltages were tested in order to determine which of them provides a better representation of the decay time. When attenuating the incident laser energy, it is clear that the decay time increases with decreasing laser energy, as could be seen earlier in Figure 5.10. Such a change in the decay time as a function of the laser energy fluence has been reported earlier for thermographic phosphors other than $CdWO_4$ [30]. When the iris was used to change the incident luminescence, a different detector response was exhibited. Data acquired at a maximum voltage output of 300mV was found to display a longer decay time than that acquired at 30 mV. This behavior is usually observed at high incident phosphorescence intensities. In Figure 5.16 b, the decay times acquired at a 300 mV output voltage level generated much shorter decay times than those acquired at 30 mV. PMT response saturation could clearly be observed, the decay times nearly half of the length of those obtained at lower output voltages (30 mV). This indicates the PMT unit here to display a much higher distortion limits at lower ranges of control voltages.

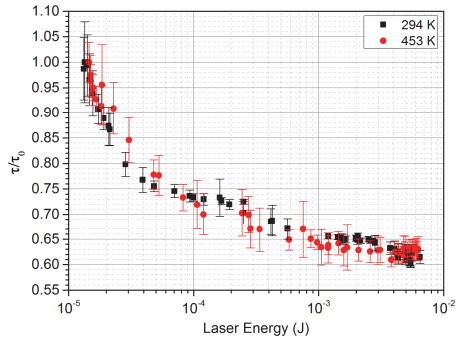


*Figure 5.17 Normalized decay times originating from CdWO4 when it is subjected to different excitation laser fluence magnitudes at 294 and at 453 K.*

All of the previously reported findings strongly suggest that the phosphorescence decay time of $CdWO_4$ is strongly dependent upon the fluence of the excitation radiation. Figure 5.17 presents a characterization of the decay time as a function of the laser energy employed for a fixed laser beam diameter. As can be seen, the decay time of $CdWO_4$ decreases with increasing laser fluence. This validates the finding that the longer decay times at low laser energies reported in **paper III** are due mainly to the effects of the laser energy involved and not to a detector-related response.

### 5.2.3 A Comparison of Time-gateable PMTs

In the investigation reported in **paper III** it was concluded that the time-gateable PMT exhibited the best performance in terms of reproduction of the phosphorescence decay waveform under various operating conditions. A continuation of the earlier study of the detector response was reported on in **paper IV**. This study involved an examination of the response of four presumably identical time-gateable PMTs (H11526-20-NF) in terms of the production type and the model involved, the specifications of the detectors in question are listed in Table 5.2.

*Table 5.2 Specifications of the individual PMTs.*

| Serial number [symbol] | Cathode sensitivity [μA/lm] | Anode sensitivity [A/lm] | Anode dark current [nA] |
|---|---|---|---|
| 58590020 [▲] | 499 | 606 | 2.1 |
| 58590039 [■] | 326 | 1490 | 6.7 |
| 58590040 [●] | 412 | 1920 | 15 |

| | | | |
|---|---|---|---|
| 58590043 [♦] | 460 | 6170 | 7.5 |
| Minimum | 350 | 350 | 10 |
| Typical | 500 | 1000 | 100 (max) |

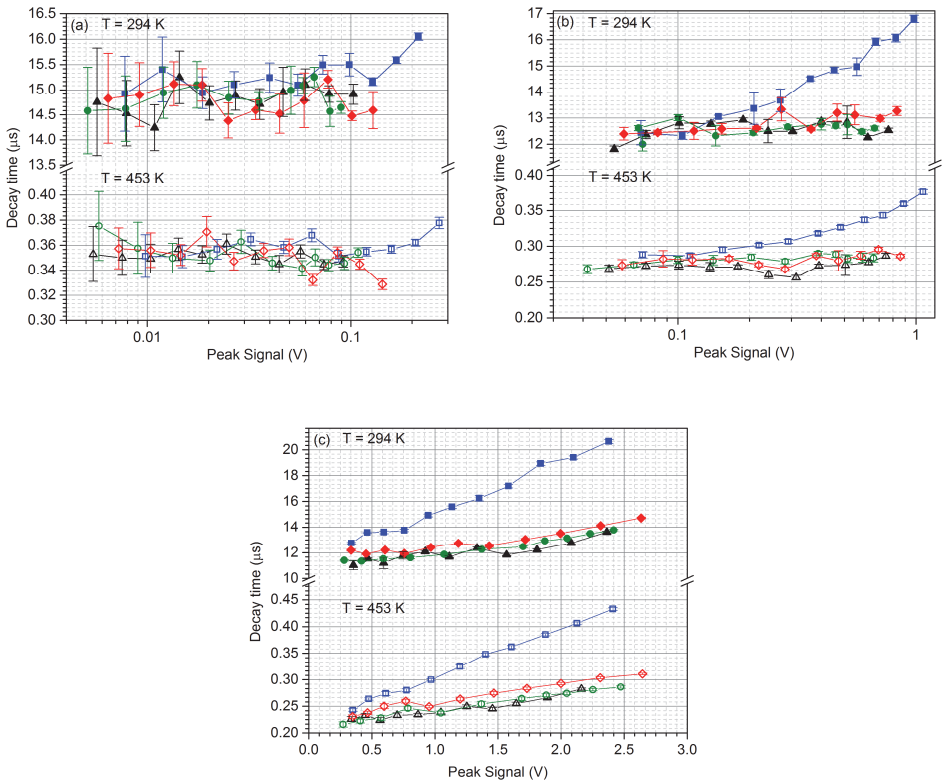


*Figure 5.18 The assessed $CdWO_4$ decay times, shown as a function of the peak output voltage of the detector as affected by variations in the control voltage of the detector when subjected to a constant light intensity for 294 K and 453 K. The markers represent the results for the H11526-20-NF PMTs listed in in Table 5.2. Each subplot was acquired at a different but constant laser energy level (20 µJ -5 mJ).*

As apparent from Table 5.2, although the PMTs in question are of the same production type, their specifications display various discrepancies. In some cases, the values of some specification (cathode and anode sensitivities) are below the minimum value or instead an order of magnitude higher than the typical value. The wide range of variations in the specifications of the PMTs indicates strongly that the response of

each unit is individual. Creating an experimental setup similar to that displayed in Figure 5.9 provided the basis for a further investigation of the individual responses obtained.

This investigation also sheds light on gain-induced distortions of the decay times obtained. Since the laser energy and incident luminescence were held constant, the effects of the electrical detector gain on the calculated decay times can be examined. The decay times were presented as a function of the maximum output voltage of the corresponding decay waveform. Figure 5.18 shows three output ranges that were obtained at each of the two different temperatures to account for the effects of the magnitude of the decay times if present. Stable decay times were found to be attained at output currents higher than those suggested by the manufacturer, of 100 μA, which corresponds to a maximum voltage output of 5 mV across a 50 Ω termination. Stable decay times were obtained up to a maximum output signal of 500-600 mV, which corresponds to a maximum current output of 10-12 mA. Figure 5.18 also shows no effect of the shorter decay times obtained at higher temperatures on the behavior of the detector.

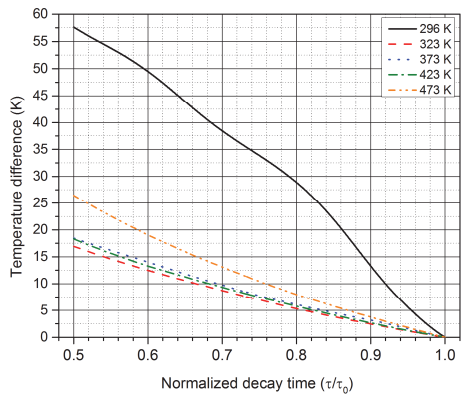


*Figure 5.19 Estimated temperature error due to decay time deviations as a function of thermographic phosphor temperature of $CdWO_4$.*

Biasing of the decay time of thermographic phosphor due to any of the possible sources of distortion affects the temperature determination process directly. In order to understand the magnitude of temperature bias due to decay time distortions, a relation has been constructed in Figure 5.19. In this figure, the difference between the true temperature and the biased temperature is estimated as a function of the deviation of the estimated from the true decay time. Since most thermographic phosphors display different levels of sensitivity across their temperature sensitivity range, it is essential that the assessment arrived at be a function of temperature as well. Depending on the temperature and the magnitude of distortions occurring, temperature deviations up to 57 K are to be expected. One should note that $CdWO_4$ is characterized by its high

degree of sensitivity, which lessens the impact that decay time related distortions have on deviations in the determined temperature. Those thermographic phosphors that show a lower decay time sensitivity to changes in temperature can be expected to exhibit greater temperature deviations in response to any distortions of their decay times that occur.

## 5.3 Lubricant-Oil Effects on the Decay Time

In using phosphor thermometry, it is important to take into consideration possible sources of distortion that could lead to erroneous temperature assessment. The investigated error sources have been those of temperature calibration and of the response of the photodetector under different operating conditions. It is of equal importance to also factor in plausible distortions originating from the experimental environment. Another possible source of distortions, if present, could affect the performance of thermographic phosphor sensors, is that of engine lubricants, the possible effects of which were subjected to a detailed inquiry in **paper V**. The present section takes up the findings, in this regard reported in **paper V**, concerning the effects of two lubricant oils that were selected (Castrol EDGE Professional V, 0W-20 and Energol CL-DX 405) have on the decay times of six different thermographic phosphors. The two lubricants were selected to cover two different areas of application, those of light-duty road transport and of large-bore marine engines, respectively. As with the detector-induced distortions reported in section 5.2, any distortions that might occur due to the presence of the lubricant oil can very well happen without this being detected by the operator. In this sense, the concealed nature of the effect calls for the enquiry regarding the effects such lubricants can have on the decay times of thermographic phosphors.

| *Thermographic phosphor* | *Temperature range[a] (K)* |
|---|---|
| $BaMg_2Al_{16}O_{27}$:Eu | 473 - 1073 |
| $BaMg_2Al_{16}O_{27}$:Eu + $Al_2O_3$ | 473 - 1073 |
| $La_2O_2S$:Eu | 293 - 600 |
| $Mg_3F_2GeO_4$:Mn | 393 - 1073 |
| ZnO:Zn | 293 - 570 |
| ZnS:Ag | 393 - 773 |

[a] Temperature range in which the decay time of the thermographic phosphor in question exhibits a sensitivity to changes in temperature.

*Table 5.3 The thermographic phosphors selected.*

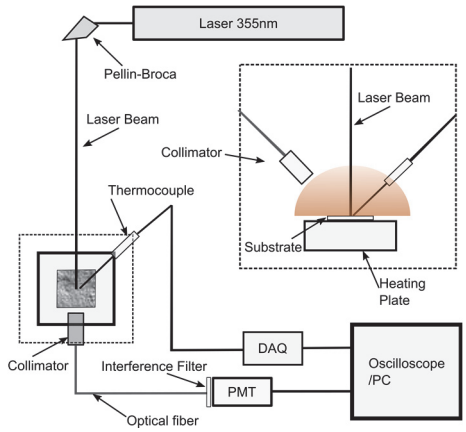


*Figure 5.20 The experimental setup used to examine the effects of the lubricant on the acquired decay time. Abbreviations: PMT (Photomultiplier tube), DAQ (data acquisition unit), PC (personal computer).*

An experimental setup was constructed to facilitate investigation of the effects of the lubricant oil in question on the decay time of each of the six selected thermographic phosphors; see Figure 5.20. The chemical composition of each of the tested thermographic phosphors along with their corresponding temperature sensitivity range are presented in Table 5.3. To eliminate any distortions produced by the detector, the electrical gain and the output voltage were held constant during the entire measurement procedure. The decay time was measured as a function of the lubricant to phosphor mass ratio as to allow for the characterization of the influence in terms of relative lubricant quantity that was present on or in the phosphor layer. The thermographic phosphors were subjected to two different temperature ranges, 294 K and 375-381 K, to examine whether or not the temperature affects the extent of the effect that the lubricant can have upon the decay time of the phosphors in question. A lubricant oil can quench the luminescence emitted by the thermographic phosphor. Quenching refers to a decrease in the intensity and decay time of the luminescence due to the interaction of the thermographic phosphor with one or more of the oil components. The investigation here concentrates on the quenching of the decay time of the phosphorescence emitted by the selected phosphors.

An examination of the spectra of the thermographic phosphors and of the lubricant oils was carried out to better understand their spectral characteristics in terms of emission and of absorption. The normalized emission spectra of the selected

thermographic phosphors after excitation of them by 355 nm laser radiation are presented in Figure 5.21. In addition, the absorption and emission spectra of Castrol EDGE Professional V, 0W-20 and Energol CL-DX 405 lubricants are illustrated in Figure 5.22. The emission and the absorption spectra indicate that there is a spectral overlap of the emission spectra of the thermographic phosphors and of the absorption and emission spectra of the lubricant oils. The greater the extent of the overlap the higher the probability of luminescence quenching due to resonant energy transfer is. This also points to the lubricants being effective absorbers of the laser UV radiation often employed to excite the thermographic phosphors. This can be problematic for thermographic phosphors that display a laser-fluence dependence of their corresponding decay time.

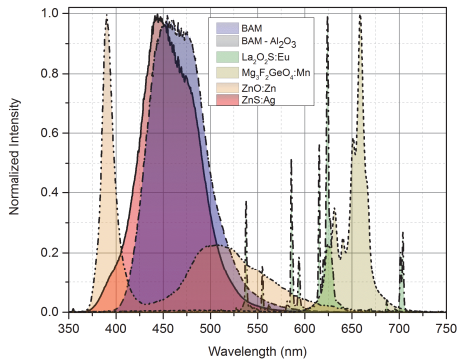


*Figure 5.21 Emission spectra of the selected thermographic phosphors under 355 nm laser radiation. $BaMg_2Al_{16}O_{27}$:Eu (dot), $Al_2O_3$ coated $BaMg_2Al_{16}O_{27}$:Eu (dash), $La_2O_2S$:Eu (dash dot), $Mg_3F_2GeO_4$:Mn (short dash), ZnO:Zn (dash dot dot), and ZnS:Ag (solid).*

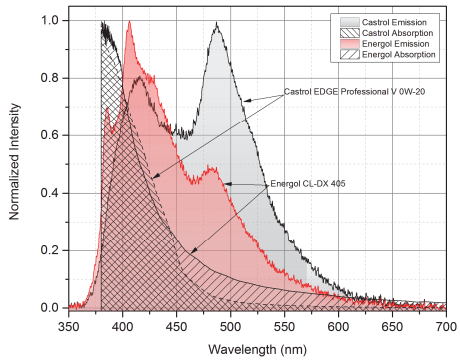


*Figure 5.22 Absorption and emission spectra of Castrol EDGE Professional V 0W-20 and Energol CL-DX 405 engine lubricants after excitation by 355 nm laser radiation.*

The reference decay times of each of the phosphors at each of the two designated temperatures were acquired. After which the lubricant was sprayed in minute quantities upon the phosphor layers and another decay time acquisition followed. This process was repeated for each of the lubricants. The ratio of the mass of the lubricant to that of the deposited thermographic phosphor layer was then used as a characterization parameter. The results obtained at 293 K, summarized in Figure 5.23 and Figure 5.24, show that only two out of the tested six thermographic phosphors, namely ZnO:Zn and ZnS:Ag, displayed a distortion of their decay time due to the presence of the lubricants. The magnitude of decay time distortion is specific to the lubricant in question and to the phosphor to which the lubricant is applied. The Energol CL-DX 405 lubricant had a much stronger effect on the decay times obtained for ZnO:Zn and

ZnS:Ag than that exhibited by Castrol EDGE Professional V 0W-20 lubricant. For lubricant/phosphor mass ratios exceeding 90 %, Energol CL-DX 405 was found to reduce the decay time of ZnOZn by a factor of 4 and that of ZnS:Ag by a factor of 35. The estimated error for the phosphorescence decay times obtained at 293 K ranged from 0.3% to 3 %. The estimated error for the lubricant/phosphor mass ratio was computed as ranging from 2 % for the highest ratios to 20 % for the lowest ratios.

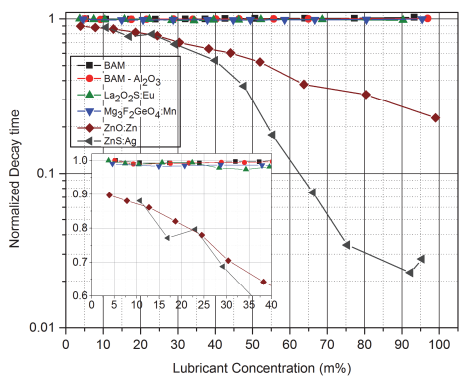


*Figure 5.23 Normalized decay time shown as a function of lubricant/phosphor mass ratio of Energol CL-DX 405 at 293 K.*

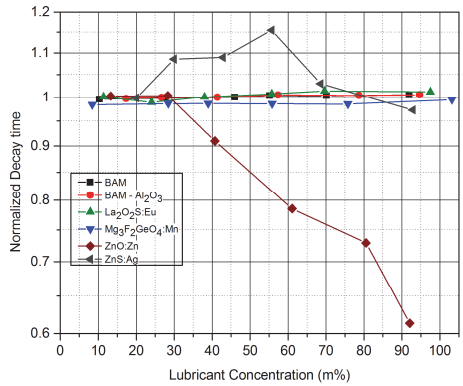


*Figure 5.24 Normalized decay time shown as a function of lubricant/phosphor mass ratio of Castrol EDGE Professional V 0W-20 at 293 K.*

The results acquired at 293 K clearly indicate both lubricants to have a strong effect on the value of the decay time obtained for some thermographic phosphors. One should bear in mind that the phosphors were kept at a constant temperature and that the detectors were subjected to identical running conditions which mean that any change in the decay time can be attributed to quenching by the applied lubricant. However, the results do not indicate how the phosphorescence that was emitted or how the decay waveform was affected. In order to shed light on the way in which the shape of the decay waveform is altered as a result of lubricant quenching, decay curves originating from ZnO:Zn and ZnS:Ag with and without the presence of Energol CL-DX 405 lubricant oil are presented in Figure 5.25. The decay curves display a strong alteration of their waveforms, and also indicate that the quenching occurred throughout the phosphor layer and not simply as a surface effect. The lubricant quenching altered the entirety of the decay curve and did not affect only a particular part of the decay curve.

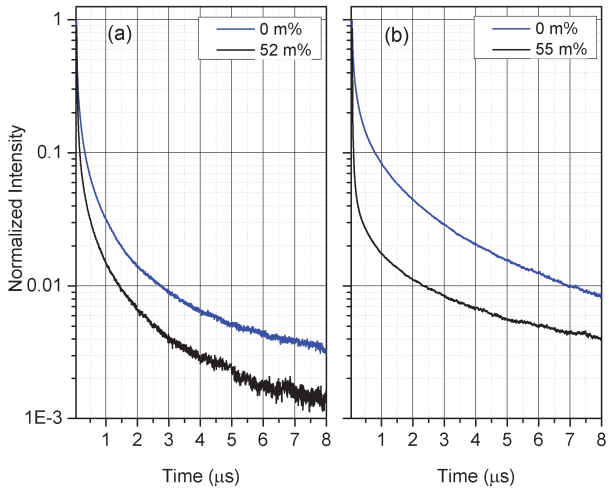


*Figure 5.25 Normalized decay curves of ZnO:Zn (a) and ZnS:Ag (b) at 293 K with and without the presence of Energol CL-DX 405 lubricant oil. The decay curves displayed are the result of an averaging of 10 single-shot decay curves.*

Tests at a higher temperature were also conducted in order to investigate whether the temperature has any impact on the magnitude of the effect that the lubricants have on the phosphorescence decay time. All of the thermographic phosphors that were tested were heated to temperatures of around 375-381 K. Heating the phosphors to temperatures higher than 400 K led to the evaporation of the lubricant oils. The results obtained also point out that ZnO:Zn and ZnS:Ag are the only thermographic phosphors of those tested that displayed a change in their decay times. It is evident, in compared with the results obtained at the two temperature levels that the temperature involved does change the magnitude of quenching effect that the lubricant has on the decay time of the phosphor which has been affected.

The decay time quenching of ZnO:Zn and ZnS:Ag thermographic phosphors that was observed can be attributed to the existence of quencher ions, such as Fe, Ni, and Co, within the lubricant oils [14, 19]. Many lubricant oils have been reported to contain these killer/quencher ions in their composition [33]. Even ppm levels of quencher ions are capable of effectively quenching the luminescence from ZnS phosphors [14]. It is also important to consider the effect of the attenuation of excitation radiation due to absorption by the lubricant oil. None of the phosphors tested manifested any sensitivity of their corresponding decay times to laser fluence. Absorption of excitation radiation by the lubricant present within the phosphor layer results in a lower level of laser fluence experienced by the thermographic phosphor layer. If a phosphor exhibits sensitivity to laser fluence in its decay time, then longer decay times are to be expected at lower levels of excitation fluence as compared to the reference decay times, as has been reported in previous studies [30, 34].

*Table 5.4 Calculated decay times of the thermographic phosphors tested at elevated temperatures when subjected to engine lubricants.*

| **Thermographic phosphor** | **BAM** | | **BAM + $Al_2O_3$** | | **$La_2O_2S$:Eu** | | **$Mg_3F_2GeO_4$: Mn** | | **ZnO:Zn** | | **ZnS:Ag** | |
|---|---|---|---|---|---|---|---|---|---|---|---|---|
| Lubricant | ***Ene.***[a] | ***Cast***[b] | ***Ene.*** | ***Cast.*** | ***Ene.*** | ***Cast.*** | ***Ene.*** | ***Cast.*** | ***Ene.*** | ***Cast.*** | ***Ene.*** | ***Cast.*** |
| Temperature (K) | 375 | | 378 | | 381 | | 375 | | 376 | | 378 | |
| Oil Conc. (m%) | 50.6 | 54.0 | 58.7 | 49.3 | 54.4 | 50.6 | 50.5 | 53.7 | 55.7 | 51.3 | 52.9 | 51.4 |
| Normalized decay time[c] | 1.03 | 1.02 | 1.02 | 1.01 | 1.01 | 0.98 | 1.02 | 1.02 | *0.22* | *0.77* | *0.69* | 0.97 |
| Normalized decay time std (%)[d] | 0.3 | 0.3 | 0.3 | 0.3 | 0.8 | 1.1 | 0.3 | 0.3 | 1.2 | 2.9 | 2.9 | 2.5 |

[a] Energol CL-DX 405

[b] Castrol EDGE Professional V 0W-20

[c] The decay times were normalized with respect to the reference decay time obtained at the same temperature without a lubricant.

[d] Standard deviation of 100 acquisition in percent

# 6 Phosphor Thermometry Technique Applications

Due to the hostility of the environments present in combustion engines, retrieving precise and accurate temperature information, or any other high-quality information, is an immense challenge. By applying phosphor thermometry to different components of a combustion engine, the temperature of these components can be determined with a high level of spatial and temporal resolution. Phosphor thermometry was applied to two different combustion engines, a large-bore two stroke marine engine and a gas turbine combustor. The temperature of the piston wall and of the burner tip was determined for each of the two engines while running under a variety of operating conditions. This section summarizes the results of studies that were carried out concerning the application of phosphor thermometry to these different types of combustion engines. The findings were published in **papers VI** and **VII**.

## 6.1 Large-bore Two-stroke Marine Diesel Engine

A section of the cylinder wall of a MAN 4T50ME-X engine was coated with $CdWO_4$ thermographic phosphor so as to retrieve the temporally resolved temperature. The engine was run in motored and fired operation modes. The specifications of the 4T50ME-X engine are listed in Table 6.1. The engine has a centrally located exhaust valve at the top of the combustion chamber and air intake ports at the bottom. The engine, of a uniflow scavenged type, is characterized by the strong swirling motion. The engine was equipped with an optical cylinder head having 24 optical ports that enables the laser radiation to be introduced and the phosphorescent signals to be retrieved from the combustion chamber. A thin layer of $CdWO_4$ thermographic phosphor was deposited on a metallic cylinder wall insert. The average thickness of the coating was measured to be around 20μm and it to have a radial spread of 55mm. A sketch of the experimental setup employed is shown in Figure 6.1.

| Engine type | 2-Stroke diesel |
|---|---|
| Number of cylinders | 4 |
| Bore [mm] | 500 |
| Stroke [m] | 2.2 |
| Stroke volume [l] | 423 |
| Compression ratio | 14:1 |
| Power [MW] | 7 |
| Max speed [rpm] | 123 |
| Max pressure [bar] | 190 |

*Table 6.1 The specifications of MAN 4T50ME-X engine.*

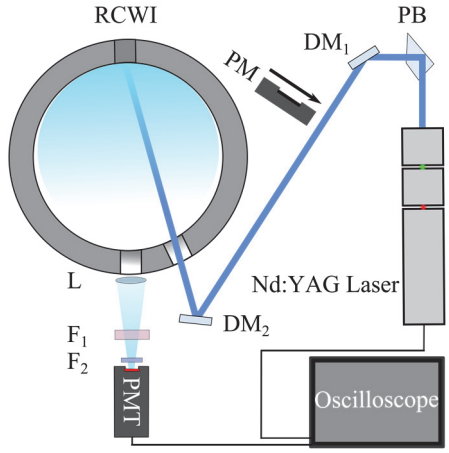


*Figure 6.1 The experimental setup for phosphor thermography on the 4T50ME-X engine. **DM**: dichroic mirror, **F1**: long-pass filter (λ>400 nm), **F2**: Interference filter (center wavelength at 450 nm, 40 nm FWHM), **L**: plano-convex lens (f = 100 mm), **PB**: Pellin-Broca prism, **PM**: laser power-meter, **PMT**: photomultiplier tube, **RCWI**: removable cylinder wall insert.*

$CdWO_4$ was excited using 266 nm radiation from an Nd:YAG laser operating at 10 Hz. Because of the marine engine having a speed ranging from 60 to 123 revolutions-per-minute (rpm), single-cycle temperature measurements could be obtained with the use of a 10 Hz repetition rate laser. Thus, a timing circuit was used to synchronize the timing of the first laser pulse with a specific crank angle degree (CAD). The remaining pulses were evenly distributed over the cycle. Depending upon the engine speed, the cycle duration could range from 0.5 to 1 second, permitting the acquisition of 5 to 9 measurements within a given engine cycle. After which the laser triggering timing was shifted to another CAD using a synchronization program. The acquisition procedure was repeated until measurements points spread over the entire combustion cycle had been acquired. The data obtained provided information concerning the temperature profile during a full combustion cycle under fixed operating conditions.

The engine was run in a motored mode, which means that the remaining three cylinders drive the test cylinder. In the motoring mode, no combustion occurs, since no fuel is injected. The resultant increase in temperature observed is due to the

compression of the air-charge loaded through the inlet ports. In this motoring phase, the driving cylinders were operated at a 12 % at 60 rpm and at a 23 % load at 75 rpm. When switching to firing operations took place, fuel (fuel oil) was injected with use of an electronically controlled injector having four injector holes. The engine was run at a 23 % at 75 rpm and at a 54 % load at 100 rpm.

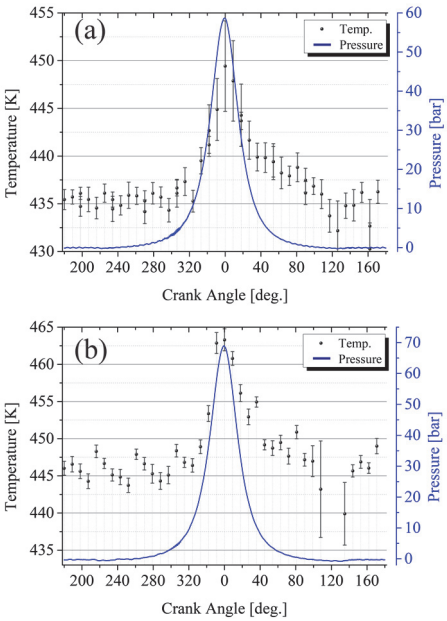


*Figure 6.2 The cylinder wall insert temperature shown as a function of crank angle degrees for motored engine operation at a driving cylinders load of **(a)** 12% (60 rpm) and **(b)** 23% (75 rpm), together with the corresponding average pressure trace.*

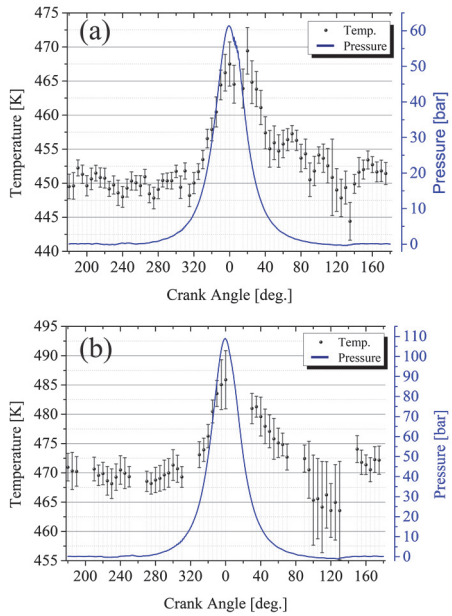


*Figure 6.3 The cylinder wall insert temperature shown as a function of crank angle degrees for fired engine operation at **(a)** a 23% load (75 rpm) and **(b)** a 54% load (100 rpm), together with the corresponding average pressure trace.*

The average temperature shown as a function of the crank angle degrees along with the corresponding average pressure trace both for motored operation and for firing operation cases are presented in Figure 6.2 and in Figure 6.3, respectively. Each data point represents the average of 50 single-shot temperatures, the error bars representing one standard deviation. As expected, the temperatures registered are higher for the firing operation mode, due to the extra energy generated by the combustion of fuel. The highest temperature registered was around 486 K for the 54 % load case. The results display the capability of the phosphor thermometry technique of providing accurate, precise, and cycle-resolved temperature information. The average standard deviation of 50 single-shot measurements was estimated to be around 2-3 K. However,

the standard deviation increased to about 8 K for crank angles located around 120 CAD after top-dead center position due to cycle-to-cycle variations. Exhaust blow down phenomenon also led to a 5 K temperature drop at around 120 CAD position, as can be seen in Figure 6.2 and in Figure 6.3.

This study indicates clearly that conducting temperature measurements can be conducted within a two-stroke marine engine through use of phosphor thermometry. These results, to the authors' knowledge, can be considered to represent the first attempt ever of applying the phosphor thermometry technique to large-bore marine diesel engines.

## 6.2 Burner-tip of Gas Turbine Combustor

The increase in temperature of the different engine components leads to a shortened longevity of components and may jeopardize the integrity of the engine. Thus, it is of considerable importance to monitor the temperature of the engine components to help maintain the integrity of the engine and prevent any catastrophic failures. Gas turbines utilize thermal barrier coatings, permitting the engine to be run at temperatures that are otherwise not possible without these coatings. Thermal barrier coatings (TBCs) are composed of ceramic materials that are characterized by their low thermal conductivity and their ability to withstand very high temperatures. By applying a layer of TBC onto an engine component, the engine component is shielded from high temperatures. This thermal shielding enables the engine to operate at higher temperatures and thus with greater efficiency. Due to lower thermal loads, TBCs also help to prolong the lifetime of the engine. The lifespan of the applied TBC layer is governed by the temperature the thermally insulating layer is subjected to, in particular the temperature of the interface between the substrate and the TBC. As the interface temperature increases, the lifespan of the TBC is significantly shortened and the probability of coating spallation becomes higher. Coating fatigue is a serious issue and TBC performance-monitoring is crucial.

TBC temperature sensing provides much-needed information for the monitoring of TBC health. However, obtaining temperature information for the interface between the substrate and the TBC layer is no trivial matter. Several reported studies have attempted to perform beneath-TBC temperature measurements using the phosphor thermometry technique [27, 35-40]. Using the same principle of luminescence detection, monitoring of the delamination and spallation of TBCs has also been achieved [36, 41-48]. There are two major deposition methods for applying the TBC layer: atmospheric plasma spray (APS) and electron-beam physical vapor deposition (EB-PVD). Due to translucence of EB-PVD coatings for UV radiation, the vast majority of studies reporting beneath-TBC temperature sensing have used EB-PVD

coatings instead of APS. APS coatings are characterized by their low UV radiation transmission or complete lack of it, and their high-scattering medium, resulting in a severe attenuation of the radiation passing through the coating. A Few studies have reported successful temperature sensing beneath an APS-deposited layer of TBC [27, 43]. These studies have established a maximum TBC thickness of around 100 µm for substrate/TBC interface temperature measurements using phosphor thermometry.

Since most TBCs are deposited in layers with thicknesses exceeding 100 µm, it is important to be able to assess the temperature of coatings similar in thickness to those used nominally in standard engines. **Paper VII** includes a study demonstrating the feasibility of conducting remote temperature sensing from beneath a 300 µm layer of APS yttria-stabilized zirconia (YSZ) TBC coating. The study consists of both a laboratory-based investigation and a temperature-sensing demonstration of a combustor burner-tip in an atmospheric rig.

### 6.2.1 Spectroscopic Investigations of Embedded Sensors and TBCs

The implementation of thermographic phosphors as embedded temperature sensors requires investigating the properties of the materials employed. Properties such as the emission spectrum, the decay time temperature sensitivity range, and possible interference from the TBC topcoat. A TBC system usually has a multi-layer structure composition. Layers such as thermally grown oxide (TGO) and the bond-coat are significant parts of such a thermally insulating system. The layer composition of the TBC system was altered here by adding two thin (less than 20 µm thick) sensing layers, as shown in Figure 6.4. The sensor materials were selected after extensive spectroscopic investigation. An experimental setup was constructed for the purpose of obtaining the necessary spectroscopic information from the sensors and the TBCs that were applied; see Figure 6.5.

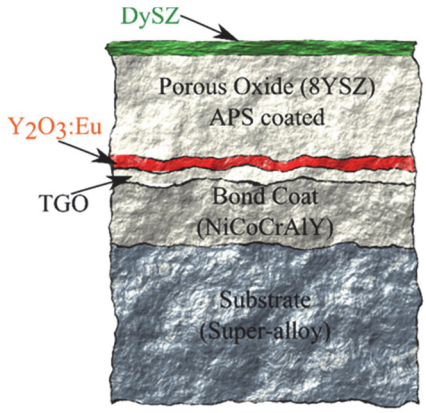


*Figure 6.4 Diagram of the TBC system, showing the added sensor layers.*

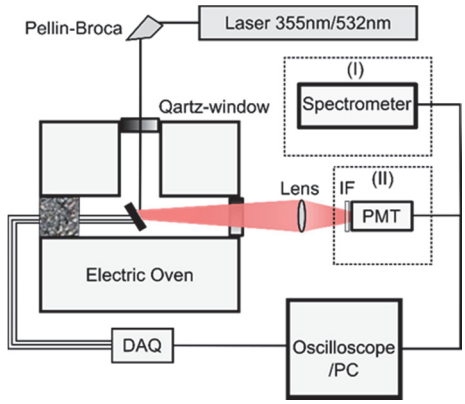


*Figure 6.5 The experimental setup constructed for studying the emission spectra and the decay time of the selected temperature sensors and the TBC materials.*

The sensors that were selected were of dysprosium–stabilized zirconia (DySZ) and Europium-doped yttrium oxide ($Y_2O_3$:Eu) which have temperature-sensing capabilities extending over the temperature range of 700 to 1300 K. As depicted in Figure 6.4, DySZ was implemented as the sensor for determining the topcoat surface temperature, Whereas $Y_2O_3$:Eu, was implemented as a sublayer sensor for the topcoat/TGO interface temperature. The choice of $Y_2O_3$:Eu as the sublayer sensor was based on the fact that $Y_2O_3$:Eu has the capability of absorbing the radiation at 532 nm that is generated by an Nd:YAG laser and that APS YSZ is partially translucent at that wavelength. Which circumvents the issue of radiation attenuation through the APS deposited YSZ topcoat layer and allows for the retrieval of the temperature sensitive luminescence.

#### *6.2.1.1 Yttria-stabilized Zirconia Topcoat Impurity Content*

Spectral interferences to signals originating from the sensor layer can hinder any possibility of performing temperature sensing. In a worst scenario, such interferences can introduce biases to the detected decay time and remain undetected throughout the temperature-determination phase. In order to test for possible spectral interferences stemming from the sprayed YSZ topcoat, five different YSZ materials were spectroscopically investigated. A list of the tested YSZ materials along with their corresponding composition, as provided by the manufacturers, is provided in Table 6.2.

*Table 6.2 List of the chemical composition and the porosity of the considered YSZ materials.*

| Product | $ZrO_2$ (m. %) | $Y_2O_3$ (m. %) | $SiO_2$ (m. %) | $TiO_2$ (m. %) | $Al_2O_3$ (m. %) | $Fe_2O_3$ (m. %) | $HfO_2$ (m. %) | Porosity (vol. %) |
|---|---|---|---|---|---|---|---|---|
| Amperit 827 | Balance | 7.0-9.0 | 0.5 | 0.4 | 0.2 | 0.3 | 2.0 | 14.6 |
| 204B-NS | Balance | 7.0-9.0 | 0.3 | 0.2 | 0.2 | 0.2 | - | 23.4 |
| 204B-XCL | Balance | 7.0-8.0 | 0.05 | 0.05 | 0.05 | 0.05 | - | 23.8 |
| 204C-NS | Balance | 7.0-9.0 | 0.7 | 0.2 | 0.2 | 0.2 | - | 18.5 |
| 204G-XCL | Balance | 7.0-8.0 | 0.05 | 0.05 | 0.05 | 0.05 | - | 20.2 |

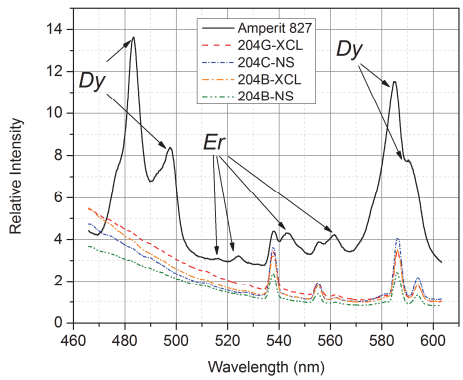


*Figure 6.6 Emission spectra of the examined YSZ materials under excitation by UV-radiation at 355 nm generated by an Nd:YAG laser.*

Figure 6.6 depicts the emission spectra obtained from each of the tested YSZ topcoats after their excitation by 355 nm radiation. The emission spectra indicate the presence of contaminants such as dysprosium (Dy) and erbium (Er). Dysprosium and erbium are not listed among the constituents of the Amperit 827 which indicates that even very low levels of impurities are sufficient to produce luminescence in YSZ materials. It has been reported in earlier studies that by doping YSZ with rare-earth elements, the YSZ becomes optically activated and can be used as a thermographic phosphor [38, 44, 49].

The remaining peaks could not be assigned to any particular element. The presence of Dy and Er in the Amperit 827 topcoat renders that YSZ material unusable

for spectroscopic applications. Since one of the sensors layers, DySZ, utilizes the temperature-sensitive luminescence from Dy, the unwanted dysprosium luminescence from the YSZ layer interferes with the dysprosium luminesce from the DySZ. Among all of the different YSZ materials that were investigated, Metco 204B-NS provides the lowest levels of emissions from contaminants. Metco 204B-NS was implemented as the topcoat for further experimentation on a combustor burner tip.

### *6.2.1.2 Dysprosium-stabilized Zirconia*

To determine the temperature sensitivity range of the DySZ (10 wt. % DySZ) sensor, the material was subjected to a spectroscopic and decay time investigation as a function of temperature. These results indicate DySZ to have the capability of providing temperature information from the decay time and the intensity ratio methods.

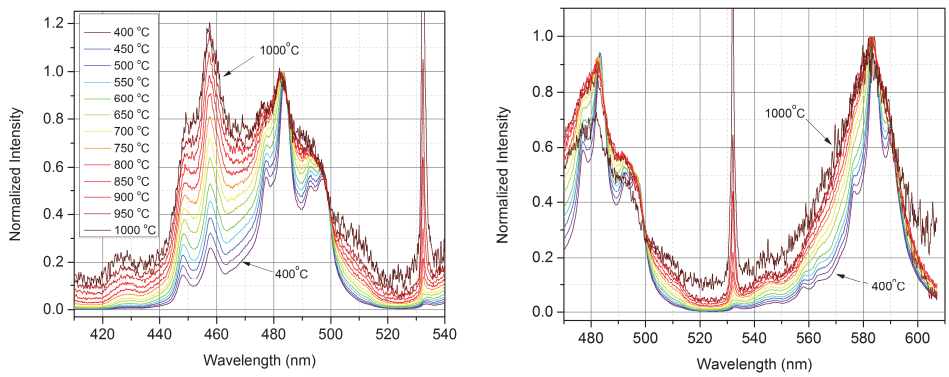


*Figure 6.7 Dysprosium-stabilized Zirconia (DySZ) emission spectra as a function of temperature after excitation by laser excitation radiation at 355 nm.*

Figure 6.7 indicates DySZ to have a high degree of spectral sensitivity as a function of temperature. Using the spectral ratio of the emission bands centered at 450 nm and 480 nm, a relation of the calculated ratio versus temperature was constructed. In addition, through use of a PMT, a decay time temperature calibration could also be constructed (Figure 6.8). DySZ was found to exhibit a temperature sensitivity range extending from 400 up to 1000 °C for both the spectral ratio and the decay time.

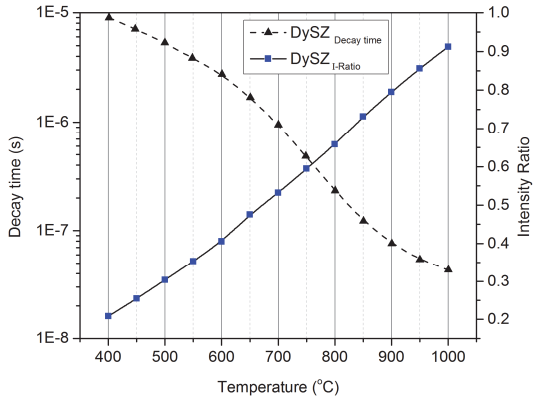


*Figure 6.8 Decay time and intensity ratio of the $I_{450}/I_{480}$, calibrations, shown as a function of temperature.*

### *6.2.1.3 Europium-doped Yttrium Oxide*

$Y_2O_3$:Eu (75 mole % Eu manufactured by Phosphor Technology) was also characterized to assess its temperature-sensing capabilities. Unlike DySZ, 532 nm excitation radiation was used to excite $Y_2O_3$:Eu. The resultant emission spectrum as a function of temperature is shown in Figure 6.9. The emission spectra distribution displays only an overall reduction in the luminescence intensity due to thermal quenching. $Y_2O_3$:Eu shows a decay time temperature sensitivity extending from 400 up to 900 °C with reduced sensitivity for temperatures above 700 °C.

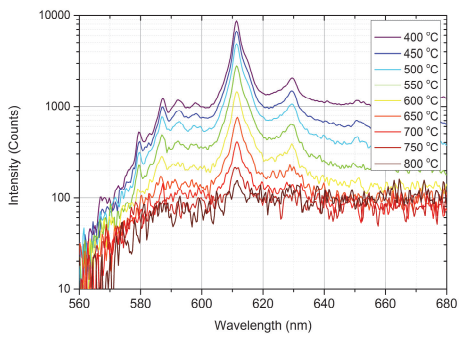


*Figure 6.9 Emission spectra of $Y_2O_3$:Eu shown as a function of temperature under beneath a 50 µm top-coat layer of 204B-NS YSZ after 532 nm laser radiation excitation.*

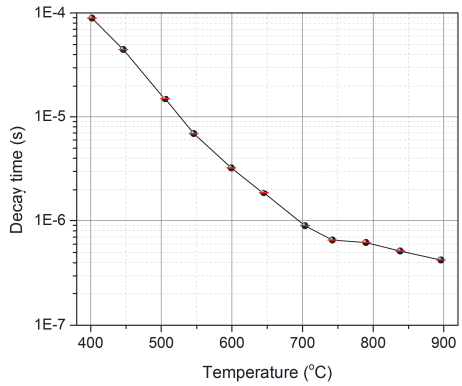


*Figure 6.10 A $Y_2O_3$:Eu calibration function after excitation by 532 nm laser beneath 200 µm of 204B-NS YSZ top-coat layer.*

### 6.2.2 Temperature Measurements of a Combustor Burner-tip in an Atmospheric Rig

After selecting sensor materials that were suitable for the objective of measuring the temperature on top and beneath a YSZ topcoat layer, a TBC system similar to that depicted in Figure 6.4 was sprayed onto the burner tip of a Siemens SGT-800 combustor. The experimental setup utilized two Nd:YAG lasers to selectively excite each of the deposited sensor layers at a specific location on TBC coated burner tip. Note that the spatial resolution of the surface temperature measurements was set by the excitation laser beam diameter. However, the expected spatial resolution of beneath-the-surface temperature measurements was lower due to excitation radiation scattering by the YSZ topcoat layer. The experimental setup employed for temperature measurements in the Siemens atmospheric test rig is shown in Figure 6.11.

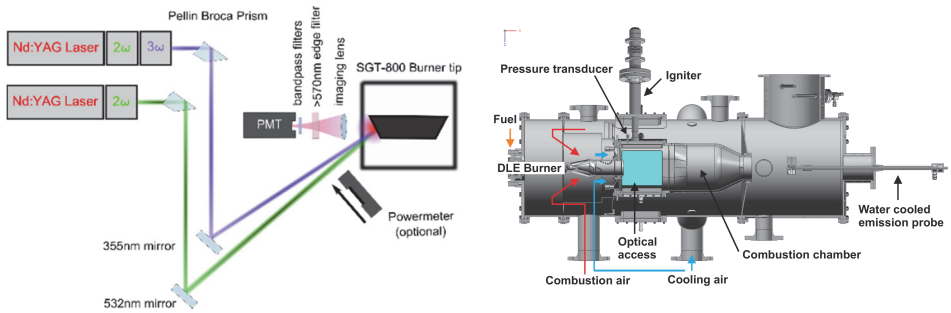


*Figure 6.11 A sketch of the experimental setup used to measure the temperature on the surface and beneath the YSZ TBC top coat together with q diagram of the Siemens atmospheric combustion test rig.*

The combustor was run through six different operating conditions. The relative pilot fuel percentage and the mean flame temperature (Ts) were changed to produce the six operating conditions selected. A list of the operating conditions that were implemented is provided in Table 6.3. The engine condition number one is considered as the reference case.

The thickness of the deposited YSZ topcoat was around 300 µm with a 20 µm DySZ layer on top of it and a 20 µm $Y_2O_3$:Eu layer beneath it. Under each of the operating conditions, a set of 200 decay curves was collected from the two sensing layers and were then processed so as to extract the decay time and consequently the temperature. The aim of the experimentation carried out was to validate the plausibility

of conducting remote temperature sensing from beneath a 300 µm thick APS coated YSZ layer. Figure 6.12 shows the normalized temperatures as evaluated from decay times originating from $Y_2O_3$:Eu sublayer, shown as a function of the engine running conditions. Temperatures obtained from a thermocouple embedded few millimeters below the metallic substrate surface close to measurement point $P_1$ are also included in Figure 6.12. The temperature profiles registered at both measurement locations, $P_1$ and $P_2$, and those registered by the thermocouple, display a similar trend as function of the engine running conditions involved. The thermocouple exhibited a lower temperature than that registered by the sensor layer due to the fact that it was embedded within the substrate. The TGO/topcoat interface temperature was found to decrease with an increase in the pilot fuel amounts.

*Table 6.3 The engine operating conditions selected.*

| Running Condition | Pilot fuel (%) | Flame Temp.(K) |
|---|---|---|
| 1 | 0 | Ts* |
| 2 | 3 | Ts |
| 3 | 6 | Ts |
| 4 | 12 | Ts |
| 5 | 0 | Ts + 100 |
| 6 | 0 | Ts + 200 |

The DySZ layer provided the topcoat surface temperature, shown here as a function of the selected engine running conditions; see Figure 6.13. The temperature was found to remain at a constant value, regardless of the operating conditions that were implemented. This temperature response, which was unexpected, can be attributed to the use of an electrical amplifier for the output signal that limited the response range of the detection system. It seems more likely that the surface of the TBC was subjected to temperatures in excess of 900 °C. The findings here indicate the possibility of obtaining temperature information from beneath a 300 µm thick APS coated YSZ topcoat layer. The dual sensing layer system that was implemented also has the ability to measure the temperature gradient across the TBC layer that was applied.

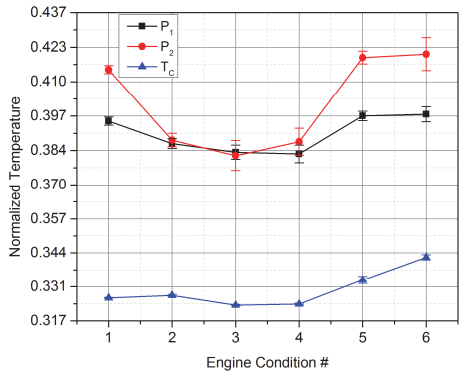


*Figure 6.12 Temperatures as determined by the $Y_2O_3$:Eu sensor at two different positions of the burner tip ($P_1$, and $P_2$) along with thermocouple temperature embedded a few millimeters beneath the substrate surface as a function of the position and the selected operating conditions.*

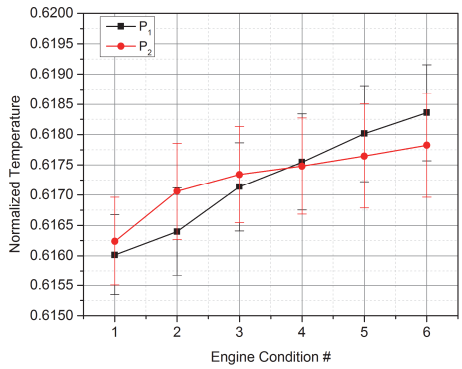


*Figure 6.13 Surface temperatures obtained by the DySZ sensor as a function of the position and the operating conditions.*

# 7 Summary and Outlook

The thesis work concerns the development and various applications of a remote laser-based temperature sensing technique known as phosphor thermometry. The developments involved here were concerned with means of achieving a greater precision and accuracy in use of the technique. This included the creation of an automatic calibration routine with a new substrate design. The devised calibration routine has the capability of continuous and automatic acquisition of a temperature calibration for thermographic phosphor of any type. The effects of the response of different detectors on the evaluated temperature were investigated. The response of the detectors was characterized in terms of the detector gain and the incident luminescence intensity the detectors were subjected to. In addition, the luminescence quenching by engine lubricant-oils of the decay time originating from several different thermographic phosphors was studied.

Two demonstrations of phosphor thermometry applications in combustion engines are also reported. The first application demonstrated remote temperature probing of the cylinder wall of a large-bore two-stroke marine diesel engine. The second application involved the integration of a dual-layer sensing system capable of providing temperature information from beneath and from the top of a TBC layer coated onto a gas turbine burner.

There is a space, however, for further improvement of the phosphor thermometry technique. The following are various points at which further investigation is needed:

- A broad selection of thermographic phosphors is available. However, for most of these thermographic phosphors information regarding their sensitivity to pressure and laser fluence is lacking. It would also be beneficial to investigate how the addition of sensitizer ions can improve the quantum efficiency and extend the saturation limit of various thermographic phosphors.
- The conclusions presented in **paper V** regarding the effects of lubricant oil on the decay time of several different thermographic phosphors, indicate the presence of quenching mechanisms that strongly affect the decay time. The mechanisms responsible for the alteration of the decay time are not completely understood and further investigations involving a broader array of thermographic phosphors and lubricants should be carried out.

- Applying phosphor thermometry in experimental environments that have a rapidly changing temperature profile necessitates the use of high speed lasers in order to temporally resolve the changes of temperature. All of the results presented here were obtained using a laser having a 10 Hz repetition rate. Utilizing a laser operating at kHz repetition rates range can significantly enhance the temporal resolution of the temperature measurements obtained. Such high repetition rates provide the possibility of obtaining cycle-resolved measurements in internal combustion engines. It also permits segment averaging within a single cycle instead of averaging over a number of different cycles.
- **Paper VII** presents an investigation of a dual layer sensing system that is capable of delivering temperature information concerning both the top of the TBC layer and the TBC/substrate interface. Further investigation is needed to examine the effects of parameters such as that of porosity changes due to TBC sintering. Extending the measurement capabilities to TBC thicknesses in excess of 300 μm is also highly desirable.
- At high temperatures, low signal levels are very common, which necessitates the use of an amplifier system to aid in the detection of very low signal intensities. Such a system introduces a bandwidth reduction to the acquisition that is possible, thus lowering the range of decay times that can be acquired by the amplified system. Employing a high-bandwidth low-noise amplifier can extend the decay time limits set by the amplifier currently being used. By increasing the system over all bandwidth, shorter decay times can be acquired, which translates directly into an extension of the maximum temperature that is measurable.

Investigation of the abovementioned matters can improve the applicability of the technique and provide improved comprehension of the parameters that can affect the performance of the phosphor thermometry technique.

# Acknowledgements

My words may fall short in expressing my gratitude and thanks to the individuals who have been there for me during my PhD studies. Excuse my shortcomings and I hope I haven't forgotten to acknowledge anyone that I had the pleasure to meet, know and work with.

My years at the Division of Combustion Physics have been nothing but thrilling. They have been a mixture of joy, new friendships, and excitement. There were some disappointments but nonetheless they enriched my experience. My journey at the Division of Combustion Physics started with a master thesis and I was lucky to have the chance then to peruse my PhD studies.

I would like to start by thanking my supervisor, Mattias Richter, for all the time and effort he invested in me. I would like also to thank him for his patience and guidance that made my PhD work a pleasant and enjoyable experience. Your passion, ingenuity, and dedication inspired me.

I also would like to thank Professor Marcus Aldén for his support throughout my studies. Thanks to Minna Ramkull for your help with all the messy certificates and documents, you are a blessing to have in this division.

Through collaboration within various projects, I had the pleasure to meet and work along with Jenny Larfeldt, Yogeshwar Nath Mishra, Johan Hult, and Andreas Lantz. Thanks to all of you for your help and enjoyable collaboration.

My gratitude also goes to my research group members who are always there for me. Joakim Rosell, you are one of the funniest guys I've met. Zheming Li, you always find hope when things go the wrong way. I wish you the best of luck with your future. Zhenkan Wang, your happy attitude is inspirational. Giota Stamatoglou, your friendship is a treasure to have. You are an amazing friend and a brilliant colleague with a vibrant laughter. Alexios Matamis, our numerous long trips to Scania and Siemens always felt much shorter with your company. Your knowledge about cars is impressive and I'm grateful for all of the amusing discussions we've had about cars.

To Per Petersson, I'm grateful to have you as an officemate. Thank you for all the support you gave me, especially the headache painkillers that eased my migraines.

Malin Jonsson, you are a great friend and travel companion. You made our trips to New York and Boston and our US road trips these a great experience.

A big shout-out to Moah Christensen who I have enjoyed talking with about 'The Walking Dead' after every episode. You give coffee and lunch break discussions an exciting and unexpected twist.

To Dina Hot, an old and dear friend who is always there for me as a listening ear and a wise advisor, your generous friendship is irreplaceable and your invaluable kind heart is unparalleled.

Jesper 'The Dude' Borggren, my best man, coffee break mate, and my best friend, we started our PhD journey together and your support has been unmatched. I cherish our friendship and I know it will last for many years to come.

Many thanks to Margita Jonis, my mother-in-law whom I regard as a second mother to me. The support you have given me has been invaluable.

To my siblings, Omar, Nour and Salah El-Dine, who endeavored through many hardships to help me get to where I have reached now, words can't suffice to express my gratitude to you.

To My Mother, Bassima, your presence in my life is a God-given blessing that I will always treasure. I would not have been able to achieve what I have achieved without your endless love and support over the years.

Last but surely not least, I would like to wholeheartedly thank you Lorraine for your patience, encouragement and unwavering love. Your tolerance of my occasional grumpiness is a testament to your unyielding dedication and care. It has been spectacular two years and I'm looking forward for a happy and wonderful lifetime with you. I do apologize for 'wasting five years not making a light saber' for you. Since now I have some time on my hands, I'm formulating a new research proposal for that. Wish me luck!

# References


[1] S. W. Allison and G. T. Gillies, "Remote thermometry with thermographic phosphors: Instrumentation and applications," *Review of Scientific Instruments,* vol. 68, pp. 2615-2650, 1997.

[2] World Health Organization. (2014). *7 million premature deaths annually linked to air pollution (World Health Organization ed.)*.

[3] World Health Organization. (2014). *Ambient (outdoor) air quality and health*.

[4] A. C. Eckbreth, *Laser diagnostics for combustion temperature and species*. Tunbridge Wells, Kent ; Cambridge, Mass.: Abacus Press, 1988.

[5] K. Kohse-Hoïnghaus and J. B. Jeffries, *Applied combustion diagnostics*. New York: Taylor & Francis, 2002.

[6] P. R. N. Childs, J. R. Greenwood, and C. A. Long, "Review of temperature measurement," *Review of Scientific Instruments,* vol. 71, pp. 2959-2978, 2000.

[7] Y. Heichal, S. Chandra, and E. Bordatchev, "A fast-response thin film thermocouple to measure rapid surface temperature changes," *Experimental Thermal and Fluid Science,* vol. 30, pp. 153-159, 2005.

[8] K. G. Kreider, "Thin film thermocouples for internal combustion engines," *Journal of Vacuum Science & Technology A,* vol. 4, pp. 2618-2623, 1986.

[9] M. A. Marr, J. S. Wallace, S. Chandra, L. Pershin, and J. Mostaghimi, "A fast response thermocouple for internal combustion engine surface temperature measurements," *Experimental Thermal and Fluid Science,* vol. 34, pp. 183-189, 2010.

[10] Y. Enomoto and S. Furuhama, "Study on Thin Film Thermocouple for Measuring Instantaneous Temperature on Surface of Combustion Chamber Wall in Internal Combustion Engine," *Bulletin of JSME,* vol. 28, pp. 108-116, 1985.

[11] L. Michalski, K. Eckersdorf, J. Kucharski, and J. McGhee, "Automatic Pyrometers," in *Temperature Measurement*, ed: John Wiley & Sons, Ltd, 2002, pp. 177-208.

[12] Hamamatsu Photonics K.K., "Photomultiplier Tubes Basics and Applications," 2007.

[13] K. N. Shinde, S. J. Dhoble, H. C. Swart, and K. Park, "Basic Mechanisms of Photoluminescence," in *Phosphate Phosphors for Solid-State Lighting*, ed Berlin, Heidelberg: Springer Berlin Heidelberg, 2012, pp. 41-59.

[14] S. Shionoya and W. M. Yen, *Phosphor Handbook*: Taylor & Francis, 1998.

[15] C. R. Ronda, "Emission and Excitation Mechanisms of Phosphors," in *Luminescence*, ed: Wiley-VCH Verlag GmbH & Co. KGaA, 2007, pp. 1-34.

[16] W. F. van der Weg, J. M. Robertson, W. K. Zwicker, and T. J. A. Popma, "Cathodoluminescence saturation effects in rare earth doped materials," *Journal of Luminescence,* vol. 24, pp. 633-636, 1981/11/01 1981.

[17] D. M. de Leeuw and G. W. t Hooft, "Method for the analysis of saturation effects of cathodoluminescence in phosphors; applied to Zn2SiO4:Mn and Y3Al5O12:Tb," *Journal of Luminescence,* vol. 28, pp. 275-300, 1983/08/01 1983.

[18] I. Syunji, Y. Shigeru, and H. Teruhiko, "Luminescence Saturation Effects in Y 2 O 2 S: Eu Phosphor," *Japanese Journal of Applied Physics,* vol. 19, p. 41, 1980.

[19] T. Masatoshi, S. Shigeo, and O. Hideki, "Mechanism of the Killer Effect of Iron-Group Ions on the Green Luminescence in ZnS:Cu, Al Phosphors," *Japanese Journal of Applied Physics,* vol. 14, p. 240, 1975.

[20] J. Lindén, C. Knappe, M. Richter, and M. Aldén, "Limitations of ICCD detectors and optimized 2D phosphor thermometry," *Measurement Science and Technology,* vol. 23, p. 035201, 2012.

[21] N. Fuhrmann, J. Brübach, and A. Dreizler, "Phosphor thermometry: A comparison of the luminescence lifetime and the intensity ratio approach," *Proceedings of the Combustion Institute,* vol. 34, pp. 3611-3618, 2013.

[22] C. Knappe, M. Algotsson, P. Andersson, M. Richter, M. Tunér, B. Johansson*, et al.*, "Thickness dependent variations in surface phosphor thermometry during transient combustion in an HCCI engine," *Combustion and Flame,* vol. 160, pp. 1466-1475, August 2013 2013.

[23] K. Yokota, S.-X. Zhang, K. Kimura, and A. Sakamoto, "Eu2+-activated barium magnesium aluminate phosphor for plasma displays – Phase relation and mechanism of thermal degradation," *Journal of Luminescence,* vol. 92, pp. 223-227, 2001.

[24] S. Zhang, T. Kono, A. Ito, T. Yasaka, and H. Uchiike, "Degradation mechanisms of the blue-emitting phosphor BaMgAl10O17:Eu2+ under baking and VUV-irradiating treatments," *Journal of Luminescence,* vol. 106, pp. 39-46, 2004.

[25] G. Bizarri and B. Moine, "On phosphor degradation mechanism: thermal treatment effects," *Journal of Luminescence,* vol. 113, pp. 199-213, 2005.

[26] K. B. Kim, K. W. Koo, T. Y. Cho, and H. G. Chun, "Effect of heat treatment on photoluminescence behavior of BaMgAl10O17:Eu phosphors," *Materials Chemistry and Physics,* vol. 80, pp. 682-689, 6/26/ 2003.

[27] J. Eldridge, T. Bencic, S. Allison, and D. Beshears, "Depth-penetrating temperature measurements of thermal barrier coatings incorporating thermographic phosphors," *Journal of Thermal Spray Technology,* vol. 13, pp. 44-50, 2004/03/01 2004.

[28] C. Knappe, K. Pfeiffer, M. Richter, and M. Aldén, "A library-based algorithm for evaluation of luminescent decay curves by shape recognition in time domain phosphor thermometry," *Journal of Thermal Analysis and Calorimetry,* vol. 115, pp. 545-554, 2014.

[29] C. Knappe, F. Abou Nada, M. Richter, and M. Alden, "Comparison of photo detectors and operating conditions for decay time determination in phosphor thermometry," *Review of Scientific Instruments,* vol. 83, pp. 094901-10, 2012.

[30] J. Brübach, J. P. Feist, and A. Dreizler, "Characterization of manganese-activated magnesium fluorogermanate with regards to thermographic phosphor thermometry," *Measurement Science and Technology,* vol. 19, p. 025602, 2008.

[31] L. J. B. Schip, B. P. Buzelatto, F. R. Batista, C. J. d. Cunha, L. C. Dias Jr., and J. B. M. Novo, "Photomultiplier nonlinear response in time-domain laser-induced luminescence spectroscopy," *Química Nova,* vol. 30, pp. 214-218, 2007.

[32] M. P. Bristow, D. H. Bundy, and A. G. Wright, "Signal linearity, gain stability, and gating in photomultipliers: application to differential absorption lidars," *Applied Optics,* vol. 34, pp. 4437-4452, 1995.
[33] E. M. Fujita, D. E. Campbell, and B. Zielinska, "Chemical Analysis of Lubrication Oil Samples from a Study to Characterize Exhaust Emissions from Light-Duty Gasoline Vehicles in the Kansas City Metropolitan Area ", Desert Research Institute, 2006.
[34] F. Abou Nada, C. Knappe, M. Aldén, and M. Richter, "Improved measurement precision in decay time-based phosphor thermometry," *Applied Physics B,* vol. 122, pp. 1-12, 2016.
[35] K. L. Choy, J. P. Feist, A. L. Heyes, and B. Su, "Eu-doped Y2O3 phosphor films produced by electrostatic-assisted chemical vapor deposition.," *Journal of Materials Research,* vol. 14, pp. pp 3111-3114, (1999).
[36] J. I. Eldridge, J. Singh, and D. E. Wolfe, "Erosion-Indicating Thermal Barrier Coatings Using Luminescent Sublayers," *Journal of the American Ceramic Society,* vol. 89, pp. 3252-3254, 2006.
[37] M. M. Gentleman, J. I. Eldridge, D. M. Zhu, K. S. Murphy, and D. R. Clarke, "Non-contact sensing of TBC/BC interface temperature in a thermal gradient," *Surface and Coatings Technology,* vol. 201, pp. 3937-3941, 12/20/ 2006.
[38] M. M. Gentleman and D. R. Clarke, "Concepts for luminescence sensing of thermal barrier coatings," *Surface and Coatings Technology,* vol. 188–189, pp. 93-100, 2004.
[39] M. M. Gentleman, V. Lughi, J. A. Nychka, and D. R. Clarke, "Noncontact Methods for Measuring Thermal Barrier Coating Temperatures," *International Journal of Applied Ceramic Technology,* vol. 3, pp. 105-112, 2006.
[40] D. R. Clarke and M. M. Gentleman, "Luminescence sensing of temperatures in thermal barrier coatings," *Surface and Coatings Technology,* vol. 202, pp. 681-687, 12/15/ 2007.
[41] J. I. Eldridge, T. J. Bencic, C. M. Spuckler, J. Singh, and D. E. Wolfe, "Delamination-Indicating Thermal Barrier Coatings Using YSZ:Eu Sublayers," *Journal of the American Ceramic Society,* vol. 89, pp. 3246-3251, 2006.
[42] J. I. Eldridge and T. J. Bencic, "Monitoring delamination of plasma-sprayed thermal barrier coatings by reflectance-enhanced luminescence," *Surface and Coatings Technology,* vol. 201, pp. 3926-3930, 12/20/ 2006.
[43] X. Chen, Z. Mutasim, J. Price, J. P. Feist, A. L. Heyes, and S. Seefeldt, "Industrial Sensor TBCs: Studies on Temperature Detection and Durability," *International Journal of Applied Ceramic Technology,* vol. 2, pp. 414-421, 2005.
[44] C. C. Pilgrim, S. Berthier, J. P. Feist, R. G. Wellman, and A. L. Heyes, "Photoluminescence for quantitative non-destructive evaluation of thermal barrier coating erosion," *Surface and Coatings Technology,* vol. 209, pp. 44-51, 9/25/ 2012.
[45] É. Copin, T. Sentenac, Y. Le Maoult, F. Blas, F. Ansart, V. Vidal*, et al.*, "Feasibility of luminescent multilayer sol-gel thermal barrier coating manufacturing for future applications in through-thickness temperature gradient sensing," *Surface and Coatings Technology,* vol. 260, pp. 90-96, 12/15/ 2014.
[46] S. Zhao, Y. Zhao, L. Zhu, L. Gu, W. Huang, X. Fan*, et al.*, "A simple non-destructive method to indicate the spallation and damage degree of the double-

ceramic-layer thermal barrier coating of La2(Zr0.7Ce0.3)2O7 and 8YSZ:Eu," *Journal of the European Ceramic Society,* vol. 33, pp. 2207-2213, 2013.
[47] L. Pin, C. Pilgrim, J. Feist, Y. Le Maoult, F. Ansart, and P. Lours, "Characterisation of thermal barrier sensor coatings synthesised by sol–gel route," *Sensors and Actuators A: Physical,* vol. 199, pp. 289-296, 9/1/ 2013.
[48] C. C. Pilgrim, S. Berthier, J. P. Feist, and A. L. Heyes, "High resolution erosion detection in thermal barrier coatings using photoluminescent layers," *Surface and Coatings Technology,* vol. 232, pp. 116-122, 10/15/ 2013.
[49] S. J. Skinner, J. P. Feist, I. J. E. Brooks, S. Seefeldt, and A. L. Heyes, "YAG:YSZ composites as potential thermographic phosphors for high temperature sensor applications," *Sensors and Actuators B: Chemical,* vol. 136, pp. 52-59, 2/2/ 2009.

# Summary of Papers

**Paper I.** **Development of an Automatic Routine for Calibration of Thermographic Phosphors**

This paper describes the development of an automatic routine for continuous calibration of thermographic phosphors. The routine developed was compared with the conventional calibration routine and was validated by the calibration of $Mg_3F_2GeO_4$:Mn thermographic phosphor. The continuous calibration routine employed included both a hardware and software elements that were developed and are described in this paper. A new substrate design using a high-performance alloy comprised the hardware elements of the presented calibration process. The software element, on the other hand, involved a real time automated acquisition system that able to simultaneously acquire the phosphor decay waveform and the thermocouple temperatures. The resultant system provided an accuracy improvement by 1-2 K and shortened the time necessary to perform a calibration by a factor of 4. The developed system was also used to investigate the magnitude of the thermographic phosphor heating as a function of the applied excitation radiation energy.

*I designed the substrate and developed the LabVIEW code controlling the different components of the acquisition system. I constructed the experimental setup, conducted the measurements, and evaluated the data. I wrote the major part of the paper.*

**Paper II.** **On the Automation of Thermographic Phosphor Calibration**

This paper represents a validation study of the calibration substrate used in the automatic calibration routine developed in paper I. Using a heat transfer model, the thermal gradients of the calibration substrate were studied in detail. The heat transfer model used a finite element method to analyze the volume under study. The heat transfer study was conducted using COMSOL software package. The results indicate there to be a maximum temperature gradient of 0.4 K within the substrate at a heating rate of 4 $K.min^{-1}$.

*I constructed the experimental setup, conducted the measurements, and evaluated the data. I also constructed the heat transfer study using COMSOL software and wrote the manuscript of the paper.*

**Paper III.** **Comparison of Photo Detectors and Operating Conditions for Decay Time Determination in Phosphor Thermometry**

This paper reports on a study of the linearity of the response of different types of photodetectors as a function of the incident phosphorescence intensity and the detector gain. A regular photomultiplier tube, a time-gated photomultiplier tube, a micro-channel plate photomultiplier tube, and an avalanche photodiode were tested. The linearity of the response detectors was characterized by the phosphorescence decay time that was measured. The effects of detector saturation were shown as a change in the measured phosphorescence decay times. Distortions of the decay times due to saturation could results in an error of tens of Kelvins in the evaluated temperatures. Experiments to investigate the saturation effects were carried out using the phosphorescence that originated from $CdWO_4$ thermographic phosphor. Tests were conducted at temperatures ranging from 290 to 580 K. Regions of linear response were identified using a detector response mapping procedure developed here.

*I constructed the experimental setup, conducted the measurements, and evaluated the data. I also contributed to the writing of the manuscript.*

**Paper IV.** **Improved Measurement Precision in Decay Time-based Phosphor Thermometry**

This paper represents a continuation of the investigations reported on in paper III. This paper also consists of a number of investigations aimed at characterizing the different sources of systematic error in temperature sensing using decay time based phosphor thermometry. The earlier investigation was concerned with the study of different types of point photodetectors. This paper, however, presents a study of photomultiplier tubes all of identical detector type for investigating the magnitude of the unit-to-unit variation in terms of the measured decay time. The study revealed that supposedly identical detectors differed in the behavior they displayed and resulted in different detector response maps. In addition, the effects of the excitation laser fluence on the decay time of $CdWO_4$ were investigated. The effects of the presence of an intense and short fluorescence peak prior to the longer and weaker phosphorescence on the measured decay time were also reported. In addition, the study also revealed that distortions originating from the oscilloscope could lead to deviations in the measured decay time.

*I constructed the experimental setup, conducted the measurements, and evaluated the data. I wrote the major part of the paper.*

**Paper V.** **Investigation of the Effect of Engine Lubricant Oil on Remote Temperature Sensing Using Thermographic Phosphors**

This paper presents a study on the potential quenching of phosphorescence from thermographic phosphors due to the presence of engine lubricant oil. The presence of the lubricant oil can affect the measured decay time and thus the calculated temperatures. The paper investigates the effects of each of two different lubricant oils on the decay time and emission intensity of six selected thermographic phosphors. Tests were conducted at temperatures around 273 and 376 K for both lubricants. It was found that only two of the tested thermographic phosphors, ZnO:Zn and ZnS:Ag, displayed an effect of the lubricant oils on their respective decay time. The remainder of the tested thermographic phosphors, $BaMg_2Al_{16}O_{27}$:Eu (BAM), $Al_2O_3$-coated $BaMg_2Al_{16}O_{27}$:Eu, $La_2O_2S$:Eu, and $Mg_3F_2GeO_4$:Mn, showed no sensitivity in their decay time to the presence of either of the two lubricant oils.

*I constructed the experimental setup, conducted the measurements, evaluated the data, and wrote the manuscript.*

**Paper VI.** **A First Application of Thermographic Phosphors in a Marine Two-Stroke Diesel Engine for Surface Temperature Measurement**

This paper presents the application of the phosphor thermometry technique to measure temperatures in a marine two-stroke diesel engine. The measurements were conducted on a MAN 4T50ME-X marine research engine equipped with an optical cylinder head. $CdWO_4$ thermographic phosphor was employed as the sensor material in these measurements. Cycle-resolved temperature measurements of the cylinder wall were obtained during motored and fired engine operation.

*I constructed the experimental setup and conducted the measurements together with Johan Hult. I was responsible for evaluating the data. I wrote the manuscript of this paper with the aid of Johan Hult.*

**Paper VII.** **Remote Temperature Sensing on and Beneath Atmospheric Plasma Sprayed Thermal Barrier Coatings Using Thermographic Phosphors**

This paper comprises investigations and measurements of remote temperature sensing on and beneath atmospheric plasma sprayed thermal barrier coatings using phosphor thermometry. The temperature of the interface between the Bondcoat and the topcoat was measured using $Y_2O_3$:Eu thermographic phosphor. Whereas the topcoat surface temperature was measured using

Dysprosium stabilized zirconia (10 wt.% DySZ) as the sensing material. Temperature measurements on and beneath the 300 µm thick layer of the yttria stabilized zirconia top-coat were successfully conducted on a Siemens SGT-800 burner in an atmospheric rig.

*I constructed the experimental setup with the aid of Andreas lantz. I conducted the measurements and evaluated the data. I wrote the manuscript with the aid of Jenny Larfeldt.*

Printed by Media-Tryck, Lund University 2016
Nordic Ecolabel 3041 0903

LUND UNIVERSITY
Faculty of Engineering
Department of Physics
Division of Combustion Physics
ISBN 978-91-7753-016-9
ISSN 1102-8718